Contents lists available at ScienceDirect

Journal of Marine Systems

journal homepage: www.elsevier.com/locate/jmarsys

Modelling suspended particulate matter dynamics at an Antarctic fjord impacted by glacier melt

Camila Neder [a,b,c,*], Vera Fofonova [c], Alexey Androsov [c], Ivan Kuznetsov [c], Doris Abele [c,1], Ulrike Falk [d], Irene R. Schloss [e,f,g], Ricardo Sahade [a,b], Kerstin Jerosch [c]

[a] Universidad Nacional de Córdoba, Facultad de Ciencias Exactas, Físicas y Naturales, Córdoba, Argentina
[b] Consejo Nacional de Investigaciones Científicas y Técnicas (CONICET), Instituto de Diversidad y Ecología Animal (IDEA), Córdoba, Argentina
[c] Alfred-Wegener-Institut für Polar und Meeresforschung, Bremerhaven, Germany
[d] Climate Lab, Institute for Geography, Universität Bremen, Bremen, Germany
[e] Instituto Antártico Argentino, Buenos Aires, Argentina
[f] Centro Austral de Investigaciones Científicas (CADIC), Ushuaia, Argentina
[g] Universidad Nacional de Tierra del Fuego, Antártida e Islas del Atlántico Sur, Ushuaia, Argentina

ARTICLE INFO

Keywords:
SPM dynamics
FESOM-C
Ocean model
Sediment
Coastal ecosystems

ABSTRACT

When Antarctic glaciers retreat, high sediment loads from geomorphological and glaciological sources can disturb the biota, especially filtering organisms, and thereby significantly alter the ecology of the Antarctic coast. We applied the Finite volumE Sea-ice Ocean-Coastal Model (FESOM-C), a numerical tool equipped with a sediment module, to simulate for the first time the suspended particulate matter (SPM) dynamics in a fjordic environment at the northern West Antarctic Peninsula, Potter Cove as a case study. Depth-averaged SPM dynamics during a meteorologically representative austral summer (120 days from December to March) considered tidal and atmospheric forcing. Additionally, idealised experiments with passive particles based on post-processing Lagrangian module identified and followed possible material trajectories in Potter Cove. Particle dynamics in the area show them to be primarily tidal and wind-driven, sensitive to bathymetry, with the higher SPM concentrations in the inner cove and the highest hydrographical complexity in the transitional area between the fjordic and marine habitat. The SPM plume covers 5.5 km^2 of the total inlet of 9 km^2, with monthly mean values between 15 and 330 mg/l. The maximum SPM concentrations are during January (790 mg/l), and the maximum plume expansion during February. The model was validated with available in situ measurements. With this study, we can identify areas in Potter Cove (and similar coastal fjordic environments, prospectively) of increasing physical stress by longer SPM residence time and high accumulation rates induced by glacial meltwater. These factors are crucial for pelagic and benthic assemblages dependent on light and food availability, as well sediment deposition.

1. Introduction

Fjords are unique and important morphological structures of glaciated coastlines. They are hotspots of marine and coastal biodiversity, highly productive systems, and recruitment areas for many marine species, including apex predators such as penguins, seals, and whales (Howe et al., 2010; Friedlander et al., 2020). These coastal ecosystems are naturally exposed to high sedimentation rates due to glacier meltwater input loaded with sediments (Thrush et al., 2004). Fjords present a clear gradient, both in environmental variables and biological assemblages towards glacier fronts, mainly driven by different sedimentation rates (Wlodarska-Kowalczuk et al., 2005; Howe et al., 2010). Under current climate changes such as increased temperatures, glacier retreat can force an increased input of terrigenous material into the fjords with a concomitant biological effect. The Antarctic Peninsula (AP) is warming faster and at a higher magnitude than the planetary mean (Hoegh-Guldberg and Bruno, 2010; Turner et al., 2016). Consequently, 90% of all tidewater glaciers on the AP coast are on retreat (Cook et al., 2016). Biological responses were predicted (Slattery and Bockus, 1997; Clarke et al., 2007; Barnes and Peck, 2008; Smale et al., 2008; Hoegh-

* Corresponding author at: ECOMARES, Instituto de Diversidad y Ecología Animal (IDEA-CONICET-UNC), Av. Vélez Sarsfield 299, 5000 Córdoba, Argentina.
E-mail address: cami.n37@gmail.com (C. Neder).
[1] Deceased

https://doi.org/10.1016/j.jmarsys.2022.103734
Received 15 September 2021; Received in revised form 8 March 2022; Accepted 15 March 2022

Guldberg and Bruno, 2010) and recent changes in benthic assemblages could be related to increased sedimentation rates in a fjord ecosystem (Sahade et al., 2015). Therefore, increased sedimentation can be considered an important forcing factor, driven by the rapid warming on the AP, in shaping Antarctic coastal ecosystems. Hence, a better understanding of the sediment input dynamics becomes crucial to improve our current predictive capacities on ecosystem responses to Climate Change.

Via subglacial and surface meltwater, polar ice sheets have the potential to alter the physicochemical properties of the oceanic water column (e.g., ocean circulation, sea-level, salinity, surface water temperature), release nutrients (e.g., silica and iron), and modify turbidity-inducing particles, contaminants, and organic carbon directly to the ocean due to fluvial erosion, hence introducing the terrestrial material into the marine system (IPCC, 2019; Meredith et al., 2019; Gutt et al., 2021). Locally enhanced freshwater run-off charged with a high concentration of lithogenic particles change the biogeochemical processes (Dierssen et al., 2002; Falk et al., 2018a; Meredith et al., 2018). An increase in turbidity results in an initial decrease of the photosynthetically active radiation in the water column and hence, in the net primary production (Schloss and Ferreyra, 2002) with consequences for local and regional food web and bentho-pelagic dynamics (Schofield et al., 2010; Braeckman et al., 2021; Gutt et al., 2021). Spatial patterns and shifts in the benthic community have been related to physical disturbance of lithogenic particles (Moon et al., 2015; Sahade et al., 2015; Pineda-Metz et al., 2019). Also, sediment run-off impacts many sensitive habitat-building and key species through light-availability reduction, shading, and sediment coverage (i.e., macroalgae, Deregibus et al., 2016), and by clogging sensitive respiratory and digestive structures (e.g., krill, Fuentes et al., 2016 or ascidians, Torre et al., 2012, 2014). Subsequently, other sediment tolerant species are locally becoming more abundant, such as bivalves (Philipp et al., 2011; Pasotti et al., 2015) or sediment dwellers such as infaunal worms (Siciński et al., 2012).

In Potter Cove, a fjord of King George/25 de Mayo Island (KGI) at the northern tip of the West Antarctic Peninsula, collaborative interdisciplinary research on the nature of coastal ecosystem has an ongoing history of over 30 years (e.g., Schloss et al., 2012; Sahade et al., 2015; Abele et al., 2017). Therefore, it serves as an ideal coastal ecosystem for assessing long-term historical climate-induced changes and predicting climate responses along the Antarctic Peninsula. Published results document the rapid landward displacement of the adjacent Fourcade Glacier (Rückamp et al., 2011; Falk et al., 2016) which has become land-terminating in 2016 (Meredith et al., 2018), except in a small portion at the north-eastern side (fig.8 from Falk et al., 2016; Deregibus and Neder unpubl.). If glacial retreat along with the AP continues leading to glaciers becoming land-terminating, the dynamics of sediment-laden meltwater and its ecological consequences we describe at Potter Cove are likely to be similar to those in most glaciated fjords around the WAP.

Falk et al. (2018a) detected daily and even hourly fluctuation of meltwater stream discharge, responding to rapidly changing weather scenarios (e.g., warm days with intense sunshine versus cold days). This illustrates the complexity of the temporal variability of the Fourcade glacial system. Periodically accelerated (Falk et al., 2016, 2018b) and episodically enhanced (Meredith et al., 2018) coastal run-off during the summer melt season alters the physicochemical regime in the water column. Monien et al. (2017) analysed the discharge of four main meltwater streams (MWS) at the south coast of Potter Cove during two austral summers (2010/11). They estimated the total suspended particulate matter (SPM) washout ranging between 23,000–39,000 tons/year for the ~9km^2 cove, albeit with highly variable sediment transport in different rivers. SPM run-off triggered a community shift from large diatoms to smaller dinoflagellate phytoplankton during the summer melt peak, affecting the pelagic food chain (Schloss and Ferreyra, 2002; Schloss et al., 2012, Garcia et al., 2019; Fuentes et al., 2016). Also, SPM run-off reduced the depth distribution of benthic macroalgal and diatom communities due to light restrictions (Zacher et al., 2007; Campana et al., 2018), and drove community assemblages' changes suggesting alternative equilibrium states (Sahade et al., 2015). Additionally, the release of ice blocks through the glacial front causes scouring of the seabed to remove benthic organisms in the shallower parts of the fjord (Deregibus et al., 2017), while in deeper areas (>10 m), sedimentation rates gain importance as a factor shaping the benthic assemblages (Lagger et al., 2018). As evidenced from the above references, in Potter Cove we are fortunate to have gathered highly resolved, multi-year knowledge of the spatio-temporal patterns of community and ecosystems shifts in response to glacier retreat (Schloss et al., 2012, 2014; Pasotti et al., 2015; Sahade et al., 2015; Jerosch et al., 2019; Braeckman et al., 2021; Lagger et al., 2021; Torre et al., 2021). This knowledge can be combined with the spatio-temporal patterns of the coastal run-off for further predictions of ecological implications at this, and other areas under glacier retreat.

The general pattern of SPM distribution in Potter Cove is a higher turbidity zone in the inner cove near the glacier front. The outer cove has more marine conditions since is less affected by glacier meltwater (Schloss and Ferreyra, 2002; Meredith et al., 2018). Jerosch et al. (2018) used a single satellite image to show a temporal snapshot for the sediment plume, which extended <1 km away from the glacier front. The geostatistical spatial analysis of Neder et al. (2020) narrows down the maximum time frame of summer SPM data to only one day. However, since local SPM is tightly linked to hydrodynamics and meteorological conditions, and is therefore highly variable (Falk et al., 2018b); the numerical reproduction of the spatial and temporal SPM dynamics remains difficult with such applied methodologies.

Understanding SPM dynamics in coastal ecosystems is crucial when (i) modelling current and future distribution scenarios of several benthic suspension-feeders and communities sensitive to sedimentation or water-mass circulation (Pineda-Metz et al., 2019), and (ii) correlating particle pathways and transport processes of dissolved substances such as nutrients or contaminants, as well organisms, i.e. pelagic larvae transport to predict and explain habitat restrictions (Jansen et al., 2018; Lagger et al., 2021; Sparaventi et al., 2021), colonisation of new ice-free areas (Lagger et al., 2017, 2018) and genetic diversification within an area (Martinez, 2021). Jerosch et al. (2018) extrapolated the local patterns of meltwater run-off and the characteristic of coastal habitats with higher sediment impact in Potter Cove to a broad area of 200–400 km^2 along King George Island's coastline, that are presently ice-covered bays and fjords. As glacial retreat remains high along the AP and is becoming land-terminating (Cook et al., 2016), there is great importance for better understanding of spatio-temporal SPM dynamics in Antarctic terrestrial to marine transition zones. Therefore, we aim to describe the transport and the spatio-temporal distribution of suspended particulate matter in the water column at Potter Cove. In particular, we will simulate: (1) the hydrodynamics applying the Finite-volumE Sea-ice Ocean Coastal model FESOM-C (Androsov et al., 2019), (2) the residence time of glacier-induced passive particles, using the Lagrangian module, and (3) the SPM concentration dynamics, equipping the model with the sediment module using as input an extensive in situ data set of meltwater and sediment discharge. These input data include sediment discharge measured in meltwater streams (Monien et al., 2017), total meltwater discharge from several glacial draining processes in Fourcade glacier sub-catchment areas (Falk et al., 2018a), run-off from meltwater streams (Falk et al., 2018b), calving (Falk et al., 2016), and groundwater discharge (Falk and Silva-Busso, 2021). Also, we will validate the SPM dynamics in Potter Cove calculating the bias of simulated and available in situ oceanographic, SPM and meteorological measurements (Roese, 1998; Monien et al., 2017; Servicio Nacional Meteorológico, 2019). We hypothesise that SPM concentration and its dynamics respond to sediment run-off budget and the velocity of residual circulation dependent on tidal and atmospheric forcing, predicting smaller bias on SPM concentration in less hydrodynamical areas and high SPM concentrations in the inner cove.

2. Methods

2.1. Potter Cove as a study area

Potter Cove, a ~ 9 km^2 fjord located at the northern part of the Antarctic Peninsula in King George/25 de Mayo Island (58° 35.0′ to 58° 41.0′ W and 62° 13.9′ to 62° 15.7′ S) has served as a long-term study area for more than three decades. Researches include observation of the rapid retreat of the Fourcade Glacier and its immediate consequences for the coastal ecology. Two central moraines divide the cove into an outer, middle, and inner part (Fig. 1). Winds control the dominating surface cyclonic circulation (Klöser et al., 1994; Schloss et al., 1997) shown by Roese (1998) and Lim (2014). The incoming water current from Maxwell Bay flows towards the middle and inner cove along the northwest coast where it then forms a gyre at the glacier front. Currents then move out to the cove along the southeast coastline at the location of the meltwater run-off streams (MWS) and Carlini station (Fig. 1).

The Fourcade Glacier discharge is measurable as freshwater and particulate inputs. These inputs are strongly related to meteorological conditions such as air-soil temperature, precipitation, and radiation that are the main drivers determining the glaciological and hydrological discharge and groundwater contribution (Fig. 1, Falk et al., 2016, 2018a,2018b; Meredith et al., 2018; Falk and Silva-Busso, 2021). Several freshwater inputs were located based on photographs taken during the summer of 2010/2011 (Fig. 2). The subdivisions of the glacier catchment were based on personal and GPS-supported observations during the annual glaciological summer field campaigns from 2010 to 2017, as well as a detailed topographic map (Braun et al., 2016). The glacier then was subdivided into smaller sub-catchments by identifying the higher glacial-elevation division accounting for gravitational flow, the position and orientation of crevasses, and the glacial flow directions (Falk et al., 2016). The derived sub-catchments (SC) were then calibrated against oceanographic data roughly quantifying the significant meltwater input to coastal waters along the coastline in Potter Cove. Subglacial discharge was acknowledged but not quantified. The total annual discharge of 25 ± 6 hm^3/y (Falk et al., 2018a) was compartmentalised into sub-catchment areas on a percentage and hourly basis (Table 1) to model in a high time resolution.

Based on the analysis of meteorological summer observations from December 1990 to February 2019 measured at Carlini station every 3 h (n = 21,763) at an altitude of 11 m (Servicio Nacional Meteorológico, 2019, Exp.175494, Argentina), we identified the summer season 2010/2011 as a representative summer to model. Mean air temperature is 1.78 ± 1.68°C, mean wind speed 34.56 ± 18.68 km/h, mean atmospheric pressure 989.1 ± 9.21 hPa and mean humidity 83.5 ± 6.9% of humidity. It is not significantly different from its previous decade mean (summers between December 2000–February 2010) of 1.84 ± 1.87°C mean air temperature, 29.20 ± 17.72 km/h mean wind speed, 989.8 ± 9.21 hPa mean atmospheric pressure and 85.5 ± 6.6% of mean humidity. Nor to the next decade mean (summers between December 2011–February 2019) of 1.04 ± 1.45°C mean air temperature, 27.91 ± 16.44 km/h mean wind speed, 984.2 ± 24.23 hPa mean atmospheric

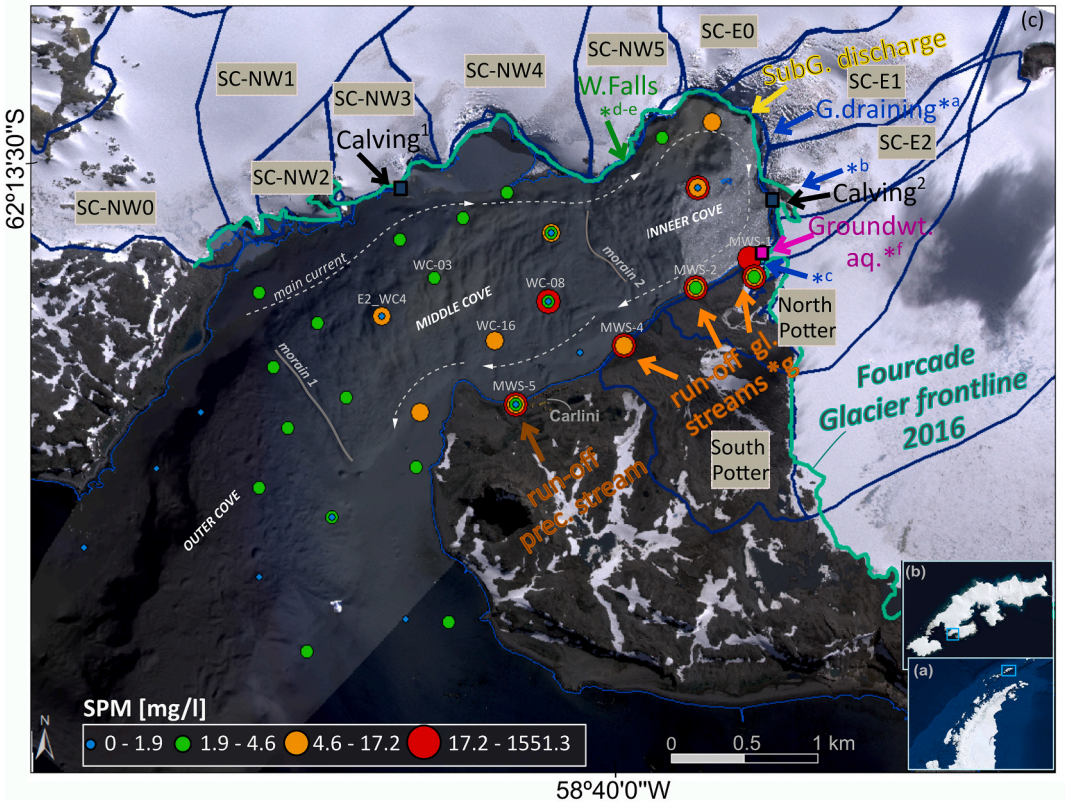

Fig. 1. Research area in Potter Cove, at the **(a)** northern tip of the West Antarctic Peninsula of **(b)** King George/25 de Mayo Island. **(c)** The Fourcade Glacier catchment is subdivided into sub-catchments (SC) from the northwest (NW) to the east (E) and the creek's catchment (North and South Potter). Glacier discharge and meltwater input processes are shown in arrows. Glaciological discharge: Glacier draining (blue arrows) and run-off glacier meltwater streams (light orange arrows); Hydrological discharge: groundwater aquifers (pink arrow), subglacial discharge, (yellow arrow) and waterfalls (green arrow); Calving: ice breaking-off front (from point 1 to 2 in black arrows). The star symbol '*' with an alphabetic character corresponds to photos in Fig. 2 and the location where they were taken. Run-off stream with precipitation origin (dark orange arrow) is not a glacier discharge but is a freshwater input. Suspended particulate matter sampling in summer 2010/2011 in increased value (mg/l) in blue, green, orange, red circles show the variation at different stations located within the cove. Meltwater streams run-off with sediment input (MWS). Background base map Maxar-DigitalGlobe (2014). (For interpretation of the references to colour in this figure legend, the reader is referred to the web version of this article.)

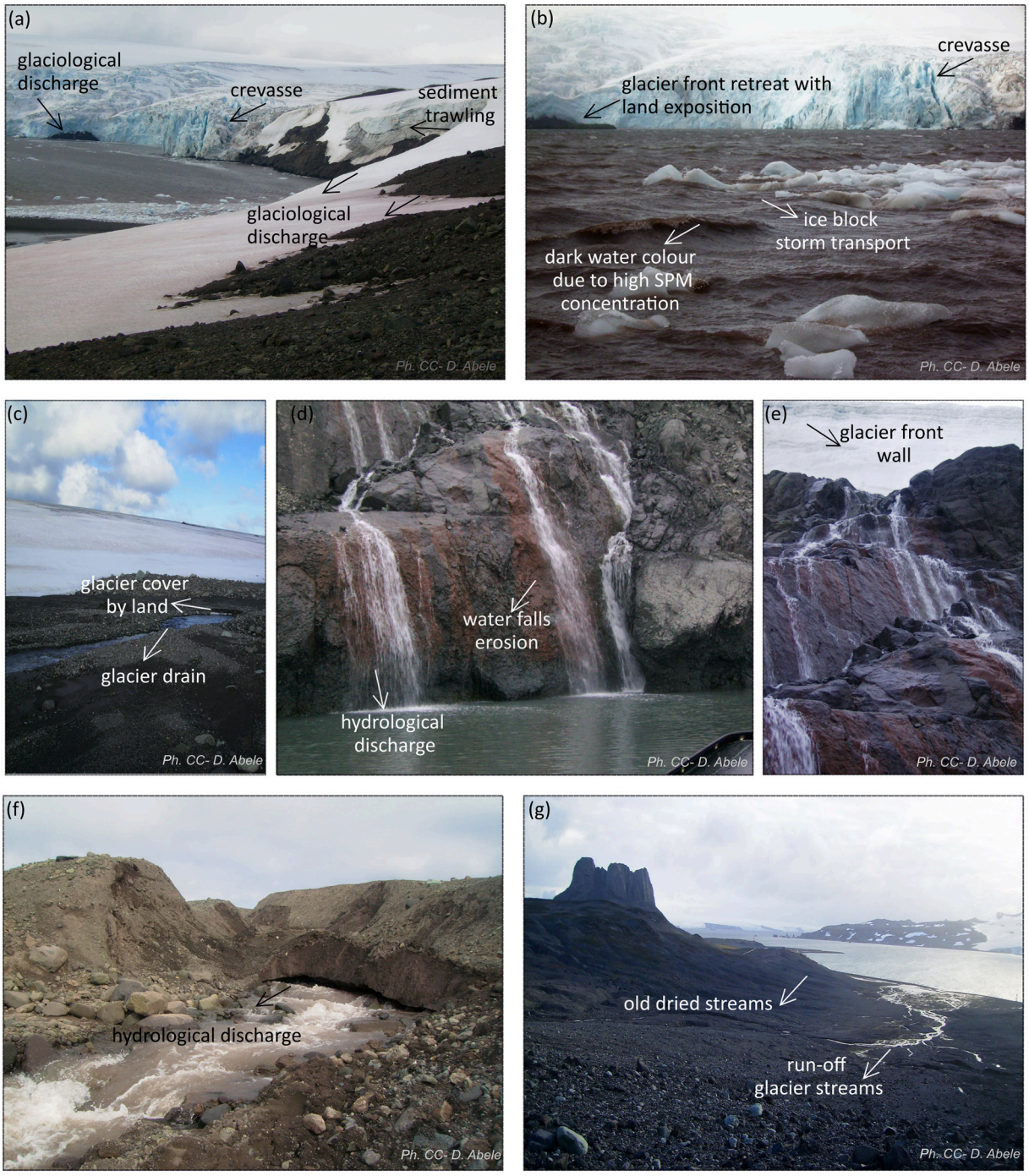

Fig. 2. During the summer season of 2010/2011 at Potter Cove, Fourcade Glacier discharge consisted of different photographed processes. Photography locations correspond to the '*' symbol in Fig. 1 following the corresponding alphabetic character **(a, b)** Glaciological discharge with glacier drains from glacier front and extensions and ice crevasse but not calving capture, Dec. 2010. **(c)** Ice-covered by land, Jan. 2011. **(d, e)** Hydrological discharge: Waterfall in the inner northern Cove with clear freshwater input, Dec. 2010. **(f)** Hydrological discharge: groundwater, Dec. 2010. **(g)** Glacier discharge: run-off streams with soil erosion dragging sediment into the Cove, entering the marine system as suspended particulate matter (SPM). Photos with Creative Common License by Doris Abele.

pressure and 90.6 ± 9.2% of mean humidity. Due to the geographic location of Potter Cove, wind direction is essential to understand the air masses and how it influences air humidity, temperature, rain. The nature of wind masses in Potter Cove differs between seasons: Westerlies during the summer with warm and moist air from mid-latitudes, Easterlies during winter with cold and dry air from the Antarctic continent (Meredith et al., 2018). Wind Rose analyses over three decades characterise Potter Cove's meteorology with a predominance of breeze type in all speed subclasses from the west and south-west (Fig. 3, Appendix A1).

2.2. FESOM-C model description

The FESOM-C model (Androsov et al., 2019) was used to simulate total SPM dynamics in Potter Cove. The FESOM-C is the coastal branch of the global Finite volumE Sea ice–Ocean Model (FESOM2; Danilov et al., 2017). The model has been validated in a series of idealised and realistic scenarios (e.g., Androsov et al., 2019; Fofonova et al., 2019, 2021; Kuznetsov et al., 2020). It uses cell-vertex finite volume discretisation and works on any triangular, quadrangular, or hybrid

Table 1
Total glacier discharge division for different processes such as glacier draining (Falk et al., 2018a, 2018b) and groundwater (Falk and Silva-Busso, 2021) considering different measurements in their maxim calculated resolution of glacier sub-catchments – SC – division and run-off meltwater streams (Falk et al., 2018b) as input in FESOM-C. Subglacial discharge remains up-to-date unknown.

Process	*Day start*	*Day end*	*Sub-catchment area*	*Long position1*	*Lat position1*	*Long position2*	*Lat position2*	*Discharge*	*Unit*	*Photographic record*
Glaciological and hydrological discharge	01/12 2010	31/03 2011	SC-NW0	−58.70843	−62.22943	−58.70626	−62.22818	7.4% of total	(m^3/h)	–
			SC-NW1	−58.70626	−62.22818	−58.70234	−62.22782	13.4% of total		–
			SC-NW2	−58.70234	−62.22782	−58.69353	−62.22693	1.3% of total		–
			SC-NW3	−58.69353	−62.22693	−58.68021	−62.22388	2.2% of total		–
			SC-NW4	−58.68021	−62.22388	−58.66065	−62.22476	11.1% of total		–
			SC-NW5	−58.66065	−62.22476	−58.64778	−62.21978	3% of total		Fig. 2 (d, e)
			SC-E0	−58.64778	−62.21978	−58.64417	−62.22016	13.1% of total		
			SC-E1	−58.64417	−62.22016	−58.63685	−62.22331	10.2% of total		Fig. 2 (a–c), Fig. 2 (f)
			SC-E2	−58.63685	−62.22331	−58.63660	−62.22752	3.5% of total		
Run-off meltwater streams	30/01 2011	05/03 2011	North Potter	−58.63660	−62.22752	−58.65155	−62.23276	1.07	(m^3/s)	Fig. 2 (g)
			South Potter	−58.65155	−62.23276	−58.65996	−62.23622	0.74		

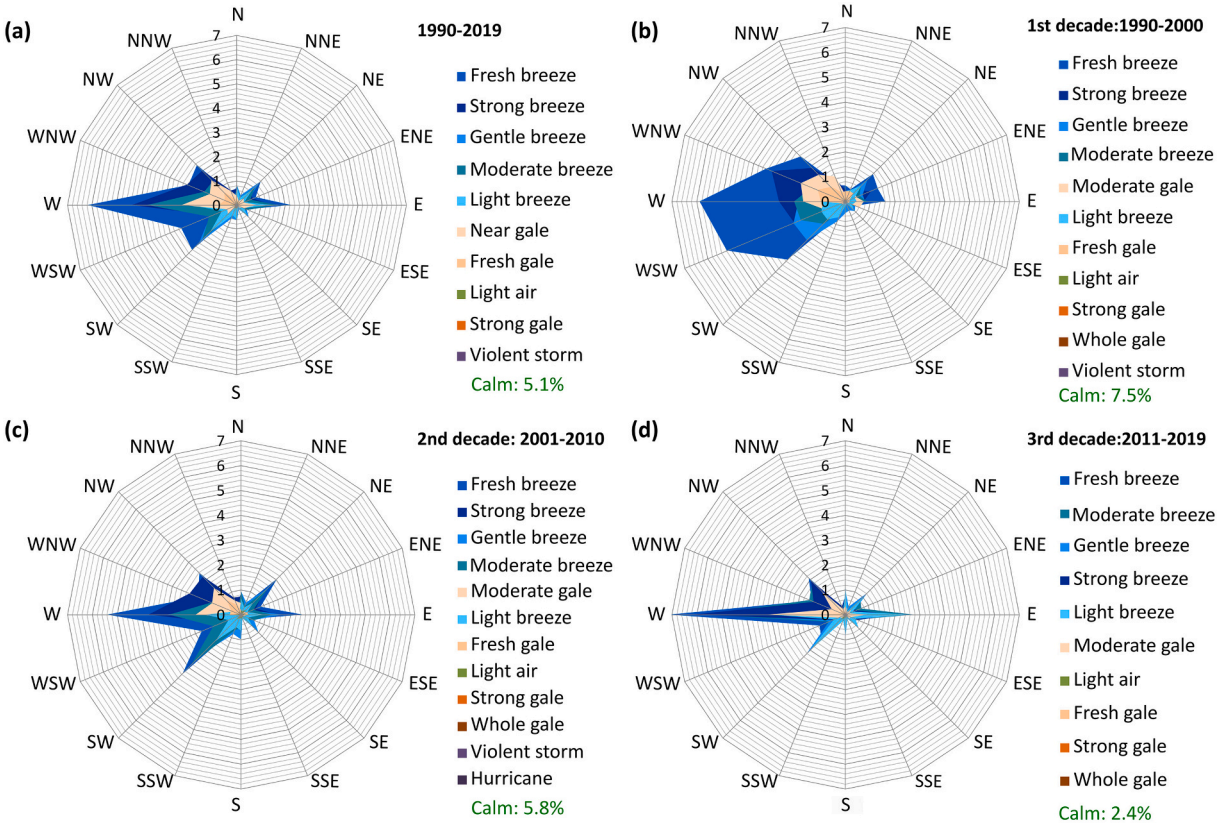

Fig. 3. Thirty years of summer wind conditions at Potter Cove. Wind roses for **(a)** all summers 1990–2019, **(b)** summers of the first decade 1990–2000, **(c)** second decade 2001–2010, and **(d)** third decade 2011–2019. The legend shows, in decreasing order, the percentage of relative wind speed frequencies classified according to Beaufort categories (Britannica, T. Editors of Encyclopaedia, 2017) for each direction. Calm wind type is extracted from the rose due to lack of direction information. For further analysis, see Appendix A. (For interpretation of the references to colour in this figure legend, the reader is referred to the web version of this article.)

meshes, ensuring geometrical flexibility and numerical efficiency for coastal simulations (Danilov and Androsov, 2015). It solves a standard set of equations for ocean dynamics in the Boussinesq, hydrostatic, and traditional approximations (see, e.g., Marshall et al., 1997).

The simulated period is one extended austral summer season from 1st December 2010 to early autumn 31st March 2011 (120 days). The SPM data availability and the representative meteorological conditions of recent summers between 2000 and 2019 dictated the period's choice. This study considers SPM as an inert stressor to the ecosystem with a higher inorganic fraction and does not consider directly biological processes such as uptake of nutrients by phytoplankton and bacteria, nutrient regeneration, or degradation. We performed a series of

barotropic 2D runs (depth-averaged solutions) with tidal forcing and turned on/off wind forcing (model setup 1, only tidal and model setup 2, tidal and wind forcing) varying parameters attributed to the sediment module. The bottom friction coefficient was set to 2.6×10^{-3}.

2.2.1. The mesh

An unstructured mesh with 30,401 nodes and 30,000 quadrilateral elements in a horizontal plane was constructed for the modelling domain using an elliptical method allowing for smooth distances between nodes and quasi-orthogonalization to the boundaries (Fig. B1). The horizontal resolution varied from 23.4 m in the deep part of the domain near the open boundary to 5.3 m in the shallow part near the coastline.

2.2.2. FESOM-C setup

Bathymetry raster in a 5 × 5 m grid (Jerosch et al., 2015; Fig. B2a) was used to define lateral solid boundary – bathymetry and coastline position of the studied domain. These data were updated to the year 2018 by a new coastline and ice-free areas in 2018, digitised from satellite imagery (DigitalGlobe, 2014, and Landsat 8 in 2018 from U.S. Geological Survey, 2019) since the most remarkable glacier retreat occurred before 2010 with a glacier retreat of 0.124 km^2 between 2010 and 2018.

We relied on the TPXO 9 atlas (TPXO, 2020; Egbert and Erofeeva, 2002) for the open boundary conditions of the tidal elevation. In this study we considered eight main diurnal and semidiurnal harmonic constituents and one higher harmonic (M2, S2, N2, K2, K1, O1, P1, Q1, M4) to generate an elevation at the open boundary. TPXO 9 atlas combines the 1/6° base global solution and the 1/30° resolution local solutions for all coastal areas, including our domain of interest. Each subsequent model in TPXO is based on updated bathymetry and assimilates more data than previously available versions (King and Padman, 2005).

The atmospheric data for our simulations were derived from downscaled re-analyses by CCLM 5.0 model (see Table 2, Zentek and Heinemann, 2020). The ocean model uses surface winds and air pressure at sea level.

The total meltwater discharge from the Fourcade Glacier catchment (Fig. B2b) defined in Table 1 for each sub-catchment depends on air-soil temperature, precipitation, and radiation, as well as variates in time from December 2010 until April 2011 (Falk et al., 2016, 2018a, 2018b; Falk and Silva-Busso, 2021. Hourly glacier discharge data were used to calculate the volume input for each sub-catchment located at the northern and eastern parts of the domain considering various glacier melt processes (Table 1 and Fig. 1). Due to a significant level of uncertainty related to the exact source location, the discharge of each sub-catchment was distributed through the whole boundary proportionally to the length of the boundary edges (Fig. B1).

SPM data for the study period were taken from the PANGAEA data archive (Neder et al., 2016), a compilation of SPM measurements from Philipp et al. (2011), Schloss et al. (2012), Monien et al. (2017), and the meteorological summer data from the Argentinian National Meteorological Service. Three meltwater streams (MWS) located in the North and South Potter creeks (Fig. 1, orange arrows), and one originating in the south-eastern part of Potter Cove (Fig. 1, brown arrow) were considered as sources of sediment discharged from the terrestrial into the marine system. The SPM concentrations were measured at these four streams hourly/daily during December 2010 and February 2011 (Fig. B2c, Monien et al., 2017). A maximum daily average input was identified on 31st January 2011 from MWS-4 (1198.1 mg/l). If the time gap between two subsequent observations were <24 h, the SPM value was linearly interpolated to generate a consistent hourly data set. Otherwise, the averaged SPM concentration was used (MWS-1: 91.1 mg/l, MWS-2: 20.1 mg/l, MWS-4: 296.6 mg/l or MWS-5: 14.8 mg/l). The freshwater run-off throughout the streams varies from 0.74 to 1.07 m^3/s (740 l/s to 1070 l/s).

Table 2
Observed and derived input data to run FESOM-C models.

Input	*Type/Resolution*	*Source*
Bathymetry	Raster data of 25 m^2 interpolated via *topo to raster* ArcGIS tool	This study, updated from Jerosch et al., 2015
Coastline	Line shapefile data	This study, updated from DigitalGlobe, 2014, Jerosch et al., 2015, U.S Geological Survey, 2019
Tidal elevation forcing at the open boundary	TPXO 9 Atlas 1/30° to force at the open boundary	https://www.tpxo.net/global/tpxo9-atlas;Egbert and Erofeeva, 2002
Coriolis pseudo-force	Value calculated at each node of the designed mesh in Potter Cove depending on the given latitude	This study
Atmospheric forcing	Downscaled reanalyses by CCLM 5.0 model with hourly resolution and 15 km horizontal resolution. Atmospheric model data linearly interpolated to the considered domain	University of Trier, CCLM simulations Weddell Sea (SPP project HE 2740/19). Pers. comm.: Günther Heinemann (Universität Trier), Zentek, Rolf (Universität Trier) and Lukrecia Stulic (AWI). Zentek and Heinemann, 2020
Glacier freshwater run-off forcing	Hourly discharge during 120 days in summer/spring (see Table 1)	Derived from Falk et al., 2016, 2018a, 2018b; Falk and Silva-Busso, 2021
Meltwater stream (MWS) SPM run-off forcing	4 MWS stations measured suspended particulate matter (SPM) concentration during nine days of summer Dec 2010 to Feb 2011 and estimated SPM percentage at the glacier front	Monien et al., 2017

Due to the lack of SPM measurements of discharge along the Fourcade glacier catchment or similar ecosystems, but acknowledging freshwater input near the glacier front along the identified sub-catchments (Figs. 1 and 2); the SPM contribution was tested. Three scenarios were proposed: the glacier discharge contained i) 0.1%, ii) 0.5%, and iii) 1% SPM of the average concentration published by Monien et al. (2017), which correspond to 0.27 mg/l (0.00027 kg/m^3), 1.35 mg/l (0.00135 kg/m^3) and 2.7 mg/l (0.0027 kg/m^3), respectively. The glacier run-off and corresponding SPM input were distributed across the whole border of each sub-catchment. Available observations evaluated the performance of these scenarios with a deviation of <0.01 mg/l at the measurements closest to the glacier front (Fig. 1, SC-NW4, SC-NW5, and E0). For this study, the middle-low glacier discharge scenario ii) of 1.35 mg/l SPM concentration (0.5%, see Section 2.5) was chosen as default due to a better performance with smaller bias in experiments with tidal and atmospheric forcing than the other two scenarios i) and iii). We should stress that additional measurements closer to the glacier front in the inner cove are needed to further confirm the number used in this study. Due to ice-breaking risks, those could not be measured. Table 2 summarises the input and forcing data to run FESOM-C modelling. Table 3 presents the output of the model.

2.3. The FESOM-C Lagrangian tracking module

As a post-processing tool, the Drift Model (FESOM-C drift) was applied to estimate the trajectories of massless particles (passive tracers) in the Lagrangian representation using the FESOM-C results. First, the horizontal velocities were interpolated to the points with the particle coordinates. Then, after calculating the velocity vector acting on the particle, its new coordinates were determined. This process was repeated. If the particle left the open boundary or remained in the same position >4-time steps (4 h), it was moved to its initial position. The drift

Table 3
Derived output from FESOM-C simulations.

Output	*Resolution*	*Source*
Sea surface height	Calculated at each node or cell centre of the designed mesh in Potter Cove. The time step in the model is 2 s. The output for all fields (as the snapshorts) is organed every hour	This study, Fig. C1
Residual circulation		This study, Fig. 4
Vorticity		This study, Fig. 5
Bottom stress		This study, Fig. C2
Current velocity		This study, Fig. C3
Tracer trajectories		This study, Fig. 7, Video S1, Fig. D1
SPM concentration dynamics		This study, Fig. 8, Video S2, Appendix E

model used calculated horizontal velocity with hourly output. Time layers for the velocity vector were linearly interpolated in one-minute increments to calculate the motion of the tracers.

A 120-days simulation (December 2010–March 2011) of a passive tracer's release experiment was carried out to understand the particle transport pattern and residence time in Potter Cove. At each particular glacier sub-catchment area, 25 tracers, and at each particular run-off MWS area, 50 tracers, were released with a radius of up to 3 grid edge lengths.

2.4. The FESOM-C sediment module

The dynamic of fine-grained sediments moving in the water column was determined based on the vertical averaged shallow water equations using: i) the equation of impurity transport with a source function describing the processes of roiling or accumulation of sedimentary material, and ii) the continuity equation written for the bottom soil in a unified system of the FESOM-C hydrodynamic model (Androsov et al., 2019). The dynamical coupling of hydrodynamics and sediment processes within the framework of one numerical model is dictated by the close relationship between litho-dynamic and hydrodynamic processes (e.g., mixing, advection), especially in the coastal areas.

The numerical model to calculate the particle transport and deposition is a set of equations defined in Androsov et al. (2019) with a source function describing the particle spatial and temporal development proportional to the difference between the actual and equilibrium concentrations in the bottom layer. Bottom sediment discharge is determined by the Van Rijn approach (van Rijn, 1984, 1985, 1987). The change in depth caused by bottom erosion or sediment accumulation was calculated based on the continuity equation, which takes the rate of settling or roiling into account. The model used assumes that the adaptation of bottom sediments to the fluid flow is instantaneous. The critical velocity of roiling was determined by the Shields criterion (van Rijn, 1984). The average settling velocity of the material available for transport was computed according to Simpson and Castelltort (2006). Each SPM simulation defined in the following section considers only one type of particle.

2.5. Sediment module evaluation

Due to the large level of uncertainty regarding the characteristics of the typical particles in the area, ten sensitivity experiments were performed to minimise the discrepancy between observation and simulation data. In a default run, the diameter of realised particles equalled 0.045 mm, particle density was set to 1450 kg/m^3, and material porosity was set to 0.4 equivalent to a mud/sand particle. In the additional experiments:

1. The particle deposition rate was decreased by 10% of the primary deposition rate.
2. The diameter of sediment particles was decreased by about 10% (from 4.5×10^{-5} m to 4×10^{-5} m).
3. The density was decreased 10%–15% of the reference density (from 1450 kg/m^3 to 1305 kg/m^3, and 1232.5 kg/m^3).

Also, we tested three sediment discharge scenarios as described in Section 2.2.2.

The model performance was evaluated by the root mean standard deviation error (RMSD) analysis between modelled and a total of 63 SPM in situ concentration measurements spatially distributed in space and time for the considered summer period and domain (Neder et al., 2016; Monien et al., 2017).

3. Results

3.1. Hydrodynamics in Potter Cove

Tidal-only forcing (setup 1) only tracks the tidal effect on the circulation pattern. The simulated residual circulation of a summary tide (by M2, S2, N2, K2, K1, O1, P1, Q1, M4 constituents) is shown in Fig. 4a. The flow reflects the bathymetric features and follows the position of the moraines, which formally divides the cove into the inner, middle, and outer cove. Note that the pattern shown represents the continuously induced tidal transport and can be treated as a benchmark circulation. This pattern does not apply to a particular time frame but represents the residual currents after one synodic month (29.5 days). It can be significantly modified by wind forcing and local currents of different origins (Fig. 4b).

The only-tidal residual circulation (Fig. 4a) differs from the residual circulation, considering both tidal and wind forcing (Fig. 4b). In the first case, the residual circulation is relatively weak with a maximum of 0.005 m/s and larger velocities in the middle cove than the inner cove. The main direction of residual circulation is cyclonic and is determined by the direction of the Kelvin wave in the Southern Hemisphere. Against the background of the main transport, there are multidirectional small-scale vortex systems of residual circulation due to the morphometric features of the modelled area and the meltwater inflow. An intensification of the residual circulation is observed as expected in the zones of large bathymetric gradient (bottom slope) where the greatest velocity shift in the spatial direction took place.

Residual velocities with the wind component showed for the whole summer 20 times higher amplitudes than in setup 1 without wind forcing, reaching 0.1 m/s. No significant changes in the velocity vectors were found in the outer cove with or without wind forcing during the considered period (Fig. C3c and d). A distinctive feature due to atmospheric forcing and bathymetry was a change in the direction of the vortex in the central deeper part (45–50 m) of the middle cove at −58.685 latitude. Noticeably, a similar circulation pattern occurred in the inner cove in both experiments, but with an intensification of the current's amplitude in the setup with wind forcing.

An important aspect of wind-driven circulation against the background of tidal dynamics was the structure of vortex fields. Monthly averaged vorticity (Fig. 5), showed high temporal variability and a complex spatial structure. Cyclonic vortices alternate with anticyclonic ones, forming a system corresponding to minimum energy loss. A cyclonic vortex along Potter Cove coastline was remarkable at the southeast coastline in January and at the northwest coast in March (Fig. 5). During December and February, the water movement followed the seafloor topography with some anticyclonic vortexes at the centre of the inner cove and in the middle cove. Both tidal dynamics and atmospheric forcing determined the character of the present vortex structures. In the middle part of the domain, the anticyclonic vortex, possibly determining the main factor in sediment transport, retained its structure throughout all months except for January. The nature of this vortex was mainly determined by the tidal movement formed during the passage of the alongshore tidal wave. The bed stress for the analysed period showed

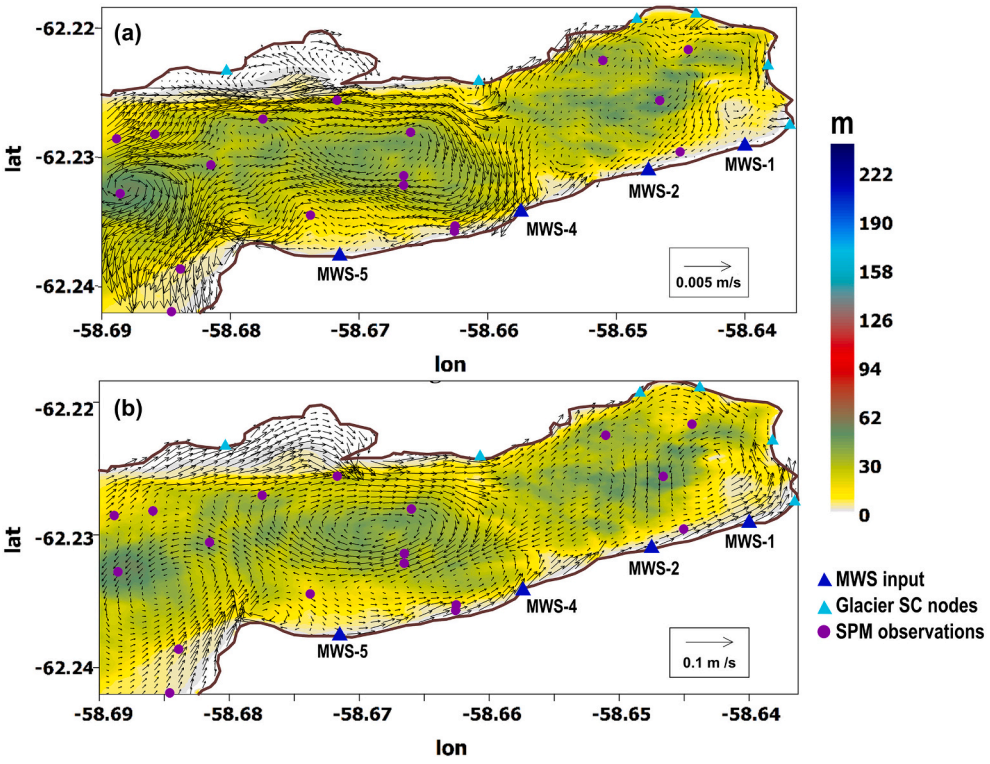

Fig. 4. Residual circulation for an extended austral summer and its velocity vectors (m/s), in Potter Cove, with **(a)** tidal forcing (setup 1) and **(b)** tidal and wind forcing (setup 2). Bathymetry in colour range (m), blue triangles show the meltwater streams (MWS) where freshwater and suspended particulate matter (SPM) run-off occur; light blue triangles delimit the glacier sub-catchments (SC) with freshwater input. Note the different scales to allow 'vector' visualisation. (For interpretation of the references to colour in this figure legend, the reader is referred to the web version of this article.)

higher values along the southern coast, leading to sediment motion of particles with small grain size as clay/silt and deposition of bigger size as sand/gravel particles (Fig. C2).

3.2. Lagrangian tracers' trajectories

As an idealised experiment, the trajectories of the massless particles (passive tracers) released from the glacier sub-catchment (SC, Fig. 6) and the four meltwater streams (MWS, Fig. 7), were calculated by the Lagrangian post-processing module. The dynamics of ten passive particles (the number of particles is limited for visualisation purposes) released from glacier SC are shown in the video 'Tracer's trajectories of glacier SC' available in the electronic version of this article (Video S1) and summarised in Fig. 6 (also see Fig. D1). Tracers stayed longer in the middle cove, and often, export from the domain occurred via the southeast coast. Note that once the particles are exported from the domain, they would be released again to restart the trajectories simulation. Particles released from SC-NW0, SC-NW1, and SC-NW2 were exported to the open sea within seven days. Particles from SC-NW3 and SC-NW4 moved in a clockwise direction towards the middle cove into the location of the moraine 2 (Fig. 6). Particles from the inner cove SC-NW4, SC-E0, SC-E1, and SC-E2 moved counter clockwise.

In the inner cove, the trajectories of the tracers released from the four MWS (Fig. 7) followed the residual circulation pattern defined by tidal and wind forcing (Fig. 4b). Such circulation retained the tracers for a longer time in the inner cove, extending the export period towards Maxwell Bay via the southern coastline. On average, the residence time of tracers was between eight days in the inner cove and three in the outer cove, with maximum residence time of 17 days (Fig. 7).

When tracers particles were released from the MWS-1, after a week the trajectories show that particles circulate in two main vortexes (yellow trajectories, Fig. 7e), one in the inner cove with a longer lifespan and the other in the middle cove with a shorter residence time before they get exported out of the domain following the southern coastline. These trajectories highlight that, particles released from this stream will likely be found in the inner cove for up to two weeks. Meanwhile, the particles released from MWS-2 will be caught in the middle cove, although the immediate circulation trajectory was towards the inner cove. Particles released from MWS-4 and MWS-5 have a shorter lifespan (between 7 and 9 days) and a faster export towards the southern coastline. Except for a single tracer, which lasted 17 days before being exported out of the domain along the north-western coastline. The experiment with the massless particles (passive tracers) allows us to follow the potential trajectories of material in the considered domain. However, a comprehensive view of SPM spatio-temporal dynamics is further described in the following section.

3.3. Suspended particulate matter dynamics

The SPM dynamics in Potter Cove during an average austral summer and beginning autumn (120 days from 1st December 2010 to 31st March 2011) was animated on an hourly basis with a spatial resolution of 5.3–24 m applied by the designed mesh. The resulting video is available in the electronic version of this article. The monthly mean of spatial SPM concentration showed an average and standard deviations of 9.17 ± 13.92 mg/l in December, 16.23 ± 17.85 mg/l in January, 17.78 ± 21.33 mg/l in February, and 14.15 ± 21.10 mg/l in March (Fig. 8a). Monthly mean SPM decreased with distance from the northern glacier front and water depth, reflecting the monthly mean vorticity (Fig. 5). Higher mean SPM concentrations (15 to >200 mg/l) were constantly found in the inner cove. The SPM plume originates from the sub-catchment area of the MWS and southeastern coastline and moves towards the inner cove in December. In January, the area with a relatively high SPM concentration starts to extend, causing a higher mean SPM concentration in the inner than in the middle cove. Subsequently, the middle cove experienced higher mean and more homogeneous SPM concentrations in February than in December (15 to >330 mg/l). The SPM input was lower in March and particles were faster exported from the cove, maintaining higher concentrations in the inner cove. MWS-1 and MWS-2 are still the main suppliers with a significant impact on the SPM dynamics (Fig. 7).

The modelled monthly average SPM plume for December, January,

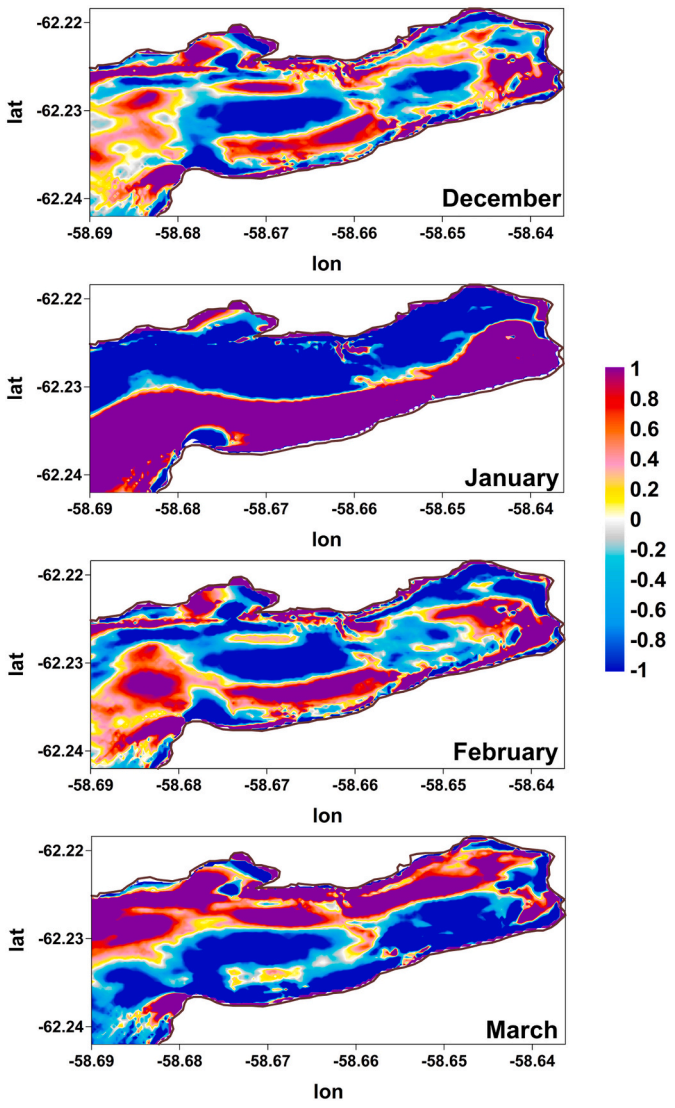

Fig. 5. Monthly mean vorticity (non-dimensional) on setup 2 (tidal and wind forcing). Positive values for cyclonic eddies and negatives for anticyclonic.

February, and March expands from the glacier front to 1.40 km^2, 3.47 km^2, 3.86 km^2, 2.51 km^2 offshore, respectively, with values between 15 and > 170 mg/l. Maximum SPM concentration occurred along the southern coast of Potter Cove with the highest estimated concentrations simulated during January 2011 of 790 mg/l SPM near the MWS run-off stations, 250 mg/l at the centre of the middle cove, and over 500 mg/l in the inner cove (Fig. E1). Contrarily, the minimum values show that during December 2010, the SPM concentration was associated directly with the MWS run-off input (Fig. E1). February 2011 concentrations were mainly derived from the particles released in the previous two weeks from MWS-1 and MWS-2 (i.e., on the 31st of January 2011) and retained in the water column of the inner cove due to atmospheric forcing.

3.4. Model assessment

According to the available sea surface height (SSH) observations, the mean sea level in the area is ~1.34 m (Fig. C1). The tidal height spectrum contains the pronounced peak at semidiurnal and diurnal frequencies attributed to tidal dynamics. The major tidal constituent was M2, with an amplitude equal to 0.43 m, followed by diurnal constituent O1 with an amplitude equal to 0.285 m based on observational data by Roese (1998). The difference between the observed and modelled amplitudes for two main constituents, M2 and O1, equalled 2.35 × 10^{-2} m and 7 × 10^{-4} m respectively, showing very good agreement between the numerical results and observational data.

Uncertainties attributed to the characteristics of the particles led us to run a series of sensitivity experiments (Table E1). The average error for all experiments was 3.74 mg SPM/l. The default configuration (Parameterization 1) resulted in the best model to describe SPM dynamics considering the smallest RMSD (root-mean-square deviation). As expected, the setup with the full forcing (setup 2) showed better results than the setup with only tidal forcing (setup 1). The RMSD for setup 1 equalled 8.5 mg/l, the RMSD for setup 2 equalled 6.5 mg/l (Table 4). The mean and maximum SPM concentration according to all available observations (n = 63) within the considered period amounted to 4.3 to 43.4 mg/l, respectively. The deviation time (Fig. 9) and spatial (Fig. 10) distribution cannot be neglected. Parameterization 2 is a remarkable example with a middle-level performance considering a RMSD of 13.9 mg/l due to the large discrepancy between simulations and observed data, particularly on 31st January 2011 at three stations in the middle-cove (WC-02, WC-08, E2-WC-04). On that day, the maximum SPM concentration was observed both in the water column and meltwater streams, and consequently, in all simulations as an overestimate between 22.6 and 66.3 mg/l. If observations of 31st January were excluded, the RMSD for all experiments varied from 3.6 to 4.8 mg/l reducing the RMSD up to 4.5 times (Table E1).

The mean deviation between the simulated and observed values per station showed better performance when the wind was included (Fig. 10a–d). Only tidal forcing bias (Fig. 10a) yielded a higher deviation with a mean underestimation of −1.35 mg/l compared to setup 2 (Fig. 10b–d, −0.55 mg/l default Parameterization 1 vs 0. 55 mg/l Parameterization 2).

A significant overestimation was evident at the stations WC-02 and WC-08, located in the middle cove, with a maximum mean bias of 3.73 mg/l in WC-02 setup 1 (Fig. 10a) and 3.84 mg/l in WC-08 setup 2 (Fig. 10b and c). Note that at these stations the average overall available observations differed by <1.3 mg/l (underestimation of 30% for WC-02 and overestimation of 27% for WC-08) excluding the measurements on the 31st of January and using a particle density of 1305 kg/m^3 (Fig. 10d). Particularly, both stations WC-02 and WC-08 in the middle cove and WC-07 in the outer cove (Fig. 10a–d) were sampled on the same critical days, the 31st January and 14th February 2011. Hence, we assume that the sources of observed bias are attributed (i) to the extreme SPM input and (ii) to the quality of the wind forcing superimposed on bathymetry data uncertainty. During 13th and 14th February, rapid changes in wind speed and direction (Fig. 11) reflected the atmospheric forcing. During 14th February, the wind from the northeast changed to the southeast and increased its velocity by six times. The velocity 2 m/s on the 13th at midnight changed to 12 m/s at ~14:00 h, shifting the current's direction towards the northwest and doubling its velocity to 0.023 m/s.

In both setups and parameterizations, a single measurement also located in the middle cove showed the highest underestimated SPM concentration by <79% of the observation (WC-16, Fig. 10). This measurement was taken on 9th February 2011, five days after a high SPM input and in the vicinity of the stations WC-02 and WC-08. The area around these stations, the middle cove, can be characterised by a more complex circulation pattern in setup 2 compared to setup 1.

On 14th February 2011, the default parameterization driven only by tides (green line, Fig. 9) performed better, indicating that rapid changes in the wind pattern have a significant effect on the currents. Fig. 12 shows the simulated currents for the dates of exceptionally overestimated SPM concentrations (13th–14th February 2011). High-speed currents along the solid boundary of the northwest and southeast coast could have led to a higher transport of particles to the middle cove during noon of the 13th February.

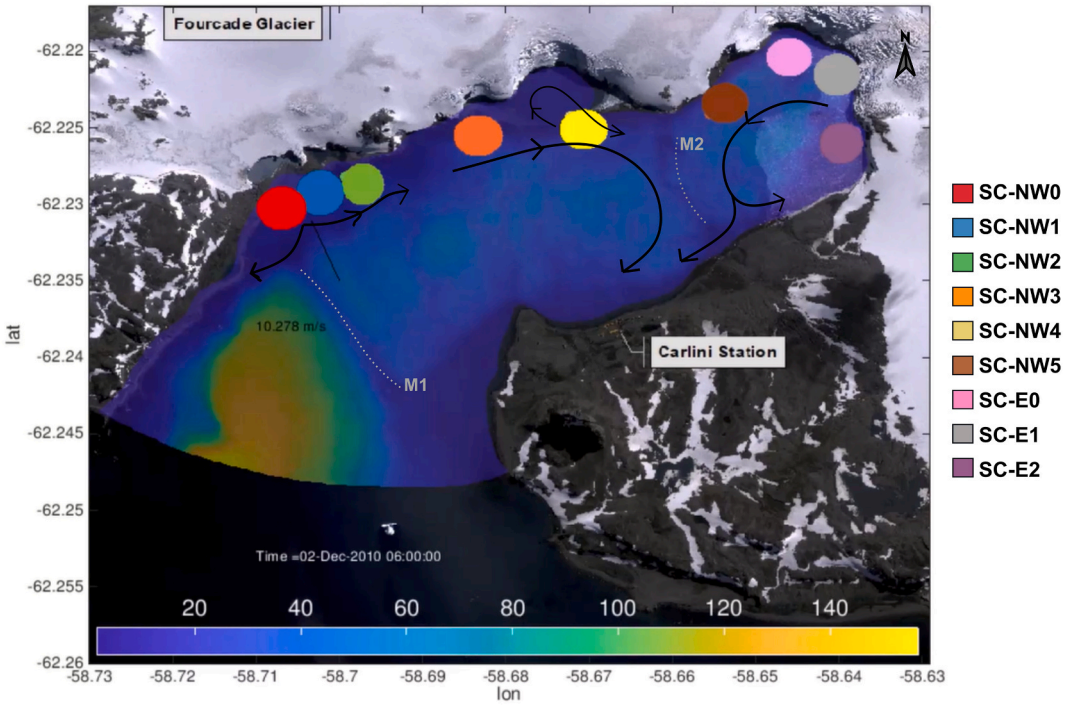

Fig. 6. Initial particle transport of massless passive tracers released from glacier sub-catchments (SC) areas shown with arrows. The dotted lines show moraines 1 (M1) and 2 (M2). The animation of the particle transport over an extended austral summer (120 days 1/12/2010–31/03/2011) is available in the electronic version of this article (Video S1).

4. Discussion

Lithogenic particle run-off into glacial coves is one of the central drivers of nearshore community change and ecosystem shift in coastal fjords (Thrush et al., 2004; Moon et al., 2015; Sahade et al., 2015; Clark et al., 2017; Braeckman et al., 2021). This modelling effort improves our understanding of the spatial and temporal distribution of SPM that influences the sessile benthic community (e.g., Philipp et al., 2011; Torre et al., 2012, 2017, 2021; Ahn et al., 2016; Campana et al., 2018; Jerosch et al., 2019). This newly-gained knowledge relates the spatio-temporal patterns of meltwater run-off to the observed ecosystem shifts in Potter Cove. It also serves as a sample study to predict future changes in comparable fjordic ecosystems along polar and subpolar regions under glacier retreat.

The results highlight that (1) the circulation pattern in Potter Cove and the consequent particle transport are driven by tidal and wind forcing sensitive to changes in wind speed and direction, and bathymetry, (2) SPM dynamics are sensitive to extreme SPM input events and SPM particle characteristics, (3) the middle cove is the area with the highest hydrographical complexity, (4) the maximum tracers residence time is 17 days with a longer lifespan in the middle cove because of the particles released from the major SPM suppliers (MWS-1, MWS-2, followed by MWS-4), and (5) the SPM plume expands in the inner and middle cove with monthly mean values between 15 and 330 mg/l with a maximum of 790 mg/l during January and a maximum plume expansion during February.

4.1. Hierarchy of drivers of coastal change

The material transport in a semi-enclosed aquatic environment is primarily determined by residual tidal circulation, which is directly related to the nonlinear processes such as advection of momentum, water level nonlinearity, and quadratic friction (e.g., Fofonova et al., 2019). Because it is the only permanent feature over time, tidally-induced residual circulation can be treated as a baseline transport force primarily driven by semidiurnal lunar constituent M2 (Androsov et al., 2019). However, as shown in this study and other coastal ecosystems, the residual circulation is sensitive to wind forcing and local baroclinic effects (e.g., Fofonova et al., 2019; Yoo et al., 2015; Ruiz Barlett et al., 2021). The model setup with tidal and wind forcing improved the model outcome by a 27% reduction in RMSD (root-mean-square deviation validated by SPM measurements) compared to the model without wind (from 8.9 mg/l to 6.5 mg/l, Table 4).

Our assumptions on the concentration and distribution of SPM from the glacier discharge (0.5% equal SPM 1.35 mg/l) resulted in a small bias (<0.01 mg/l) between observed and modelled values comparing the variation of the three possible scenarios. Deviations occurred mainly due to high SPM input during critical days (31st January and 14th February, Monien et al., 2017) when rapid changes in wind speed and directions changed the currents and delayed the response in the sediment plume of up to five days (9th February, Neder et al., 2020). The SPM observations do not always capture the extreme measurements when weather conditions do not allow navigation. Additional run-off measurements of the glacier catchment and closer to the glacier front would contribute to improving the model.

We observed that SPM dynamics were highly sensitive to particle characteristics. Particles of lower density (from default 1450 kg/m^3 to 1305 kg/m^3) doubles the RMSD when the critical date of the maximum input (31st January) was included. Meanwhile, a decrease in the particle diameter (4.5×10^{-5} m to 4.0×10^{-5} m) improved the overall performance by 5–16%, reducing the RMSD when data measured at that date were not included. These changes in performance indicate that the dominant particles suspended in the water column could consist of a pool of particles with a mixture of densities and sizes. The organic and inorganic fraction of the SPM might behave differently as the organic matter is smaller (<2 μm). This corresponds with the finding that lighter clay particles correlated with the organic fraction are horizontally transported, forming the SPM plume. Meanwhile, the silt fraction mostly sinks to the bottom (Schloss et al., 1999).

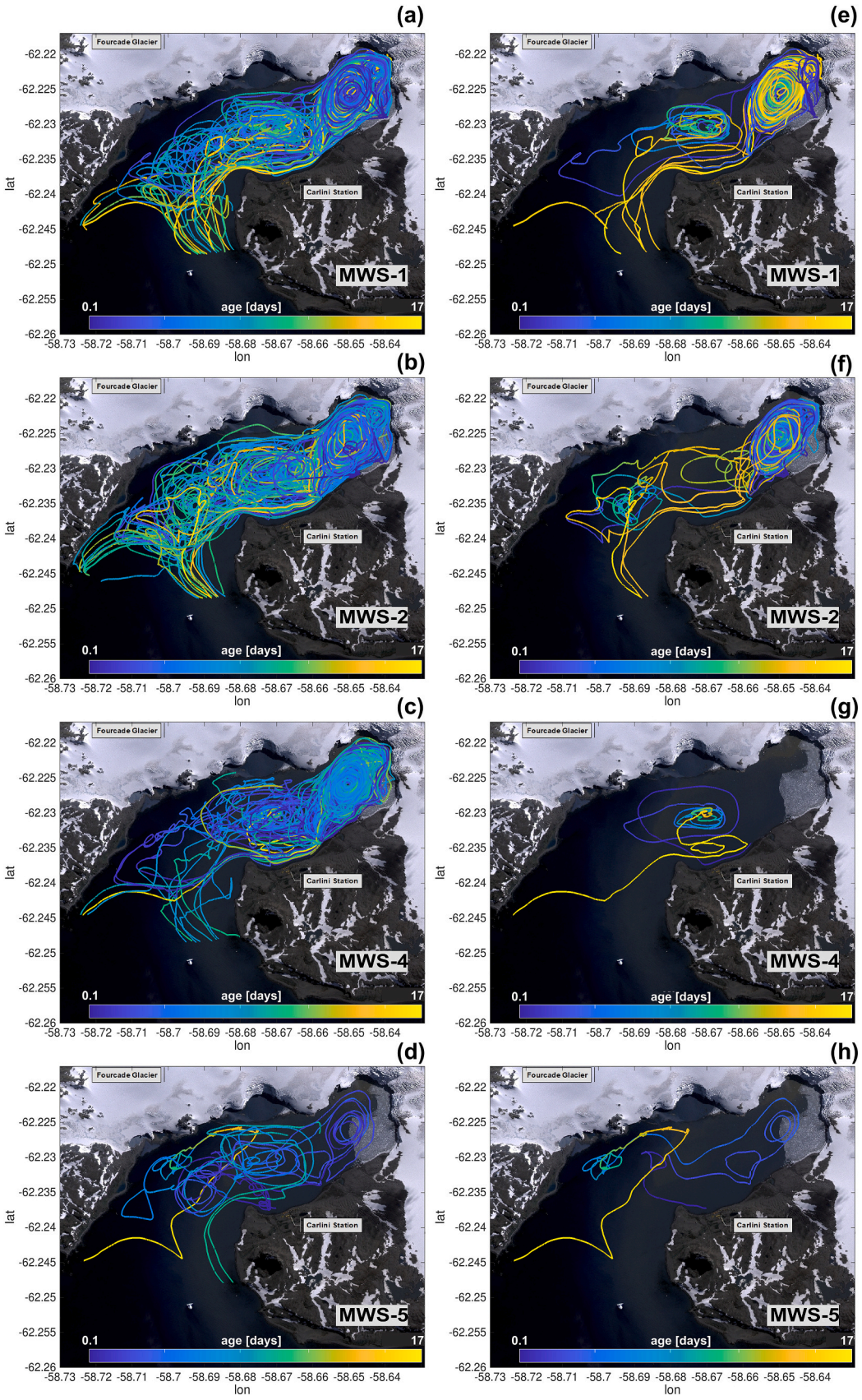

Fig. 7. Trajectories of those passive tracers released from the four run-off meltwater streams (MWS) in Potter Cove with a lifespan of more than **(a–d)** one week and **(e–h)** two weeks after release, respectively.

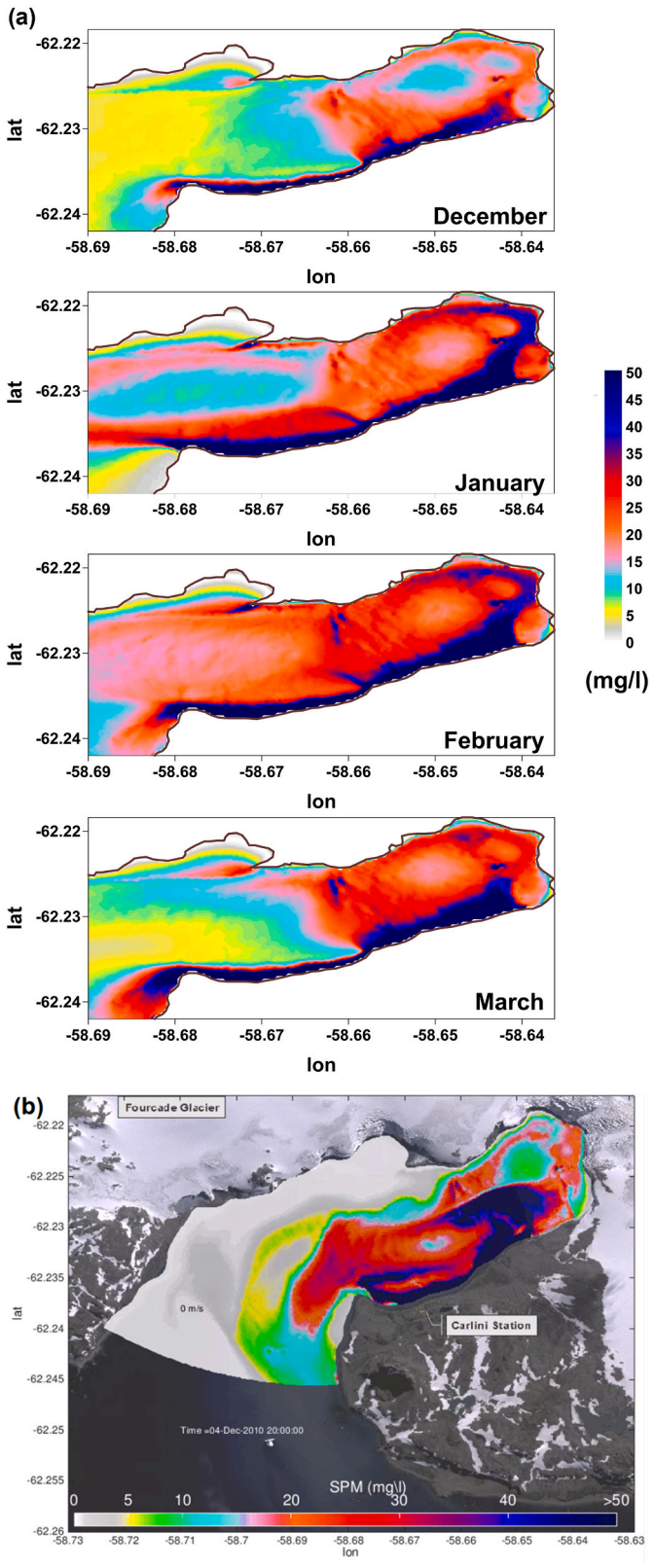

Fig. 8. **(a)** Suspended particulate matter (SPM) plume expansion and average monthly concentration simulated for December 2010 until March 2011. Considered particles have 4.5 × 10^{-5}m diameter and 1305 kg/m^3 density. **(b)** SPM dynamics is available in the electronic version of this article (Video S2).

4.2. SPM spatial-temporal distribution

This is the first model simulating SPM dynamics in Potter Cove. A model animation showing results is available in the electronic version of this article (Fig. 8b). The present analysis of 120 days SPM distribution with high temporal (hourly) and spatial resolution (meters) show a complex and dynamic picture in Potter Cove. The SPM dynamics ranged from 0.02 to >330 mg/l, in agreement to Monien et al. (2017) spatial summer estimation. In particular, the spatial mean SPM concentration pattern estimated for a summer scenario proposed by Monien et al. (2017) is comparable with the maximum values simulated for February in our analysis. The local circulation patterns and the SPM dynamics show the middle cove to be the area of highest hydrographical complexity. This area represents a transition between the inner cove, highly affected by meltwater and sediment input, and the marine habitat. Following Neder et al. (2020)'s range of high SPM values between 4 and 35 mg/l, the dynamic SPM plume reaches a monthly average area of 5.02 km^2 and expands it an additional 0.5 km^2 with SPM concentrations >35 mg/l.

The hydrography of Potter Cove, the dynamic expansion of the SPM plume, and the classification based on the cluster analysis by Jerosch et al. (2018), indicates that the meltwater fjord habitat can be reclassified. On one extreme, the meltwater fjord habitat could be extended to a wider area (monthly mean 5.52 km^2) by merging with the fjord habitat (FH). A more conservative approach (Fig. 13), would be to reclassify the now-single benthic habitat into four: high meltwater fjord habitat (HMFH) up to moraine 2, low meltwater fjord habitat (LMFH) up to the deepest area of the centre of the middle cove, fjord habitat (FH) up to moraine 1 and marine habitat (MH).

The SPM simulations of this study and the plume spread of lithogenic particles transported into marine systems are consistent with observations in other marine studies. At the North Sea (51°–52°N), the plume varies similarly to our study along the gradient from the SPM source to the marine habitat unaffected by the discharge, showing sediment concentrations near the coast between a minimum of 20–70 mg/l with maxima up to 1000 mg/l, to a minimum of <10 mg/l in the offshore area (Fettweis et al., 2007). Our monthly SPM mean values are slightly higher than those measured in the Arctic Kongsfjorden Fjord (79°N 12–13°E) where SPM concentrations range between 0.13 and 8.38 mg/l (Ardini et al., 2016). Also, SPM values are two orders of magnitude lower (50–14,200 mg/l) than the maximum-SPM simulated concentrations in the Canadian Arctic (68°–70°N, 138–132°W) during the boreal summer 2010. Such difference could be attributed to the SPM budget considered to be transported by the Mackenzie River, characterised as the river that transport more lithogenic particles to the Arctic Ocean than any other Arctic River (Doxaran et al., 2012). As in the Potter Cove middle area, Doxaran et al. (2012) and Fettweis et al. (2007) highlight higher variations of the SPM in the transitional area between turbid rivers, plumes, and particles in open ocean conditions.

4.3. Beyond SPM dynamics: ecological implications

If the regional warming trend at the Antarctic Peninsula continues as predicted (IPCC, 2019; Meredith et al., 2019), we can envision two non-exclusive scenarios related to the effects of tidewater glacial retreat on coastal ecosystems such as Potter Cove: (i) initially, increased glacial meltwater discharge with high sediment load from the underlying moraine in the glacier foreland or (ii) then the streams eventually dry out and meltwater SPM transport ceases.

The tracer dynamics (Fig. 7) show that particles transported by the meltwater streams closer to the glacier front (MWS-1 and MWS-2) are retained in the inner cove during a longer period compared to those MWS further away from the glacier. Particles transported by MWS-4 are tracked in the inner cove within the first week. Potential scenarios can be described if the glacier continues retreating at high speed (1.7 m/y to the glacier front reference point in 2018). On one side, the increase in air

Table 4
Root-mean squared deviation (RMSD) in mg/l error for selected numerical experiments with best performances: default Parameterization 1 and Parameterization 2. Mean and maximum observations for the whole period, including measurements on a high SPM input date (31st January) and without them.

	Incl. 31st of Jan, N of obs. = 63	*w/o31st of Jan, N of obs. = 57*	*Diameter size of the SPM (m)*	*Density of the SPM (kg/m^3)*	*Settling velocity (%)*	*SPM scenario (mg/l) (i) 0.27 (ii) 1.35 (iii) 2.7*
Parameterization 1 (tidal forcing only)	8.9	4.4	4.5×10^{-5}	1450.0	100	(ii)
Parameterization 1 (tidal and wind forcing)	6.5	4.3	4.5×10^{-5}	1450.0	100	(ii)
Parameterization 2 (tidal and wind forcing)	13.9	4.3	4.5×10^{-5}	1350.0	100	(ii)
Mean obs., (mg/l)	4.3	3.7				
Max. obs., (mg/l)	43.4	37				

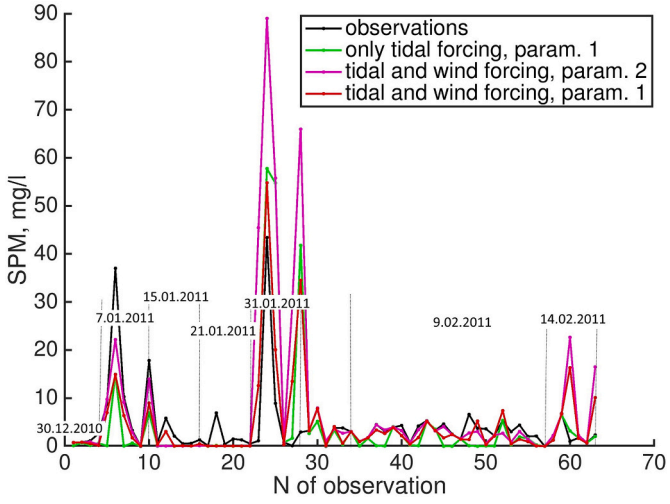

Fig. 9. Intercomparisons of the two selected Parameterisations of numerical experiments with tidal only forcing (setup 1) and tidal and wind forcing (setup 2). Note the higher bias between observations on 31st January followed by 14th February 2011, and simulated suspended particulate matter (SPM) in mg/l.

temperature could induce an increase of meltwater streams with higher proportions of lithogenic particles carried into the fjord, with a longer lifespan in the inner cove but moving inside the entire cove. Further, the particle concentration depends on the type of bedrock beneath the glacier that is being scraped away. If glaciers retreat exposes sedimentary bedrock, which is a porous rock and therefore particularly sensitive to erosion, warming will accelerate the increase of subglacial sediment run-off. However, if glacial retreat uncovers erosion-resistant basalt, there may be a decrease in sediment input once the glacier has completely retreated overland. On the other hand, if the glacier retreats quickly, it could result in creating a high terminal moraine that hampers a further run-off into the fjord. Consequently, SPM concentrations may decrease.

A certain threshold in sediment concentrations can trigger an abrupt change in the ecosystem (Sahade et al., 2015; Torre et al., 2021). Because the sedimentation process influences community compositions based on species-specific physiological perturbation thresholds (Torre et al., 2014, 2021), a decline or increase in SPM concentrations could shift the system to a new alternative equilibrium state. Torre et al. (2021) estimated the scope for growth of three ascidians species increase up to 10 mg/l and become negative between 40 and 60 mg SPM/l, values ranged at the ecosystem in the present study.

The SPM concentrations simulated in the inner cove and along the southern coastline could explain observed spatial and structural shifts in the benthic community. Species sensitive to sedimentation, such as ascidians (Sahade et al., 2015; Torre et al., 2021) or practically unaffected by it like the soft-coral *Malacobelemnon daytoni* by Lagger et al. (2021) would be highly vulnerable. In the case of this soft-coral, the analysis of its distribution has been related to a time-lag on the exposition of the ice-free area (Lagger et al., 2021). The fact that the particles remain in the middle cove and the gyre limits the transport towards the inner cove could explain the time-lag of the species with a pelagic phase to colonize a newly-available habitat. Our results about circulation pattern and the post-processing Lagrangian analysis of passive tracers can contribute to the understanding of the pelagic system, such as larvae pathways from the middle cove to the inner cove, as well the benthic spatial distribution pattern explained through water circulation and variables related to water-mass characteristics (Pineda-Metz et al., 2019). Therefore, our study provides the baseline for further modelling sediment-sensible species distribution and system shifts under changing environmental circumstances. These are crucial hints considering that species survival and biological community shifts can affect carbon standing stock potential for sequestration, and consequently, the negative feedback on climate change (Barnes et al., 2020; Zwerschke et al., 2021).

Suspended particulate matter also decreases light penetration through water, shallowing the compensation point for primary production thus reducing phytoplankton biomass accumulation in Potter Cove (Schloss and Ferreyra, 2002; Schloss et al., 2012). SPM further affects zooplankton and, in particular, krill, as shown in Fuentes et al. (2016). Garcia et al. (2019) showed the influence of glacier-related particles on other zooplankton causing a transition from an herbivorous to a microbial-based food web in proximity to the glacier and particle-induced perturbation. Along with the coastal areas around KGI, Jerosch et al. (2018) calculated that an additional 200–400 km^2 could be similarly affected by glacier influence.

King George/25 de Mayo Island is often outside the dry and cold areas of the polar vortex, even during winter since the global climatological circulation patterns are changing and modifying the extension of the circumpolar vortex around Antarctica (Meredith et al., 2019). The consequences are that glacial melt and retreat are enhanced, as well as loss and melt of permafrost (Falk and Silva-Busso, 2021). Even if the current warming trend is reversed (Falk et al., 2018a), melting will continue until the glacier reaches its equilibrium. Freshwater release modifies the local circulation patterns in fjords ecosystems through subglacier release from tidewater glaciers and run-off from land-terminating glaciers (Meredith et al., 2019). The Potter Cove system is a prime example of both processes and their ecological consequences allowing to generalise responses to climate change along with other polar and subpolar ecosystems.

5. Conclusion

We provide SPM dynamics resulting from the application of coastal ocean model FESOM-C to a unique data set of sediment run-off data measured at meltwater streams, in the water column, and from glacier discharge through several draining processes in glacier sub-catchment

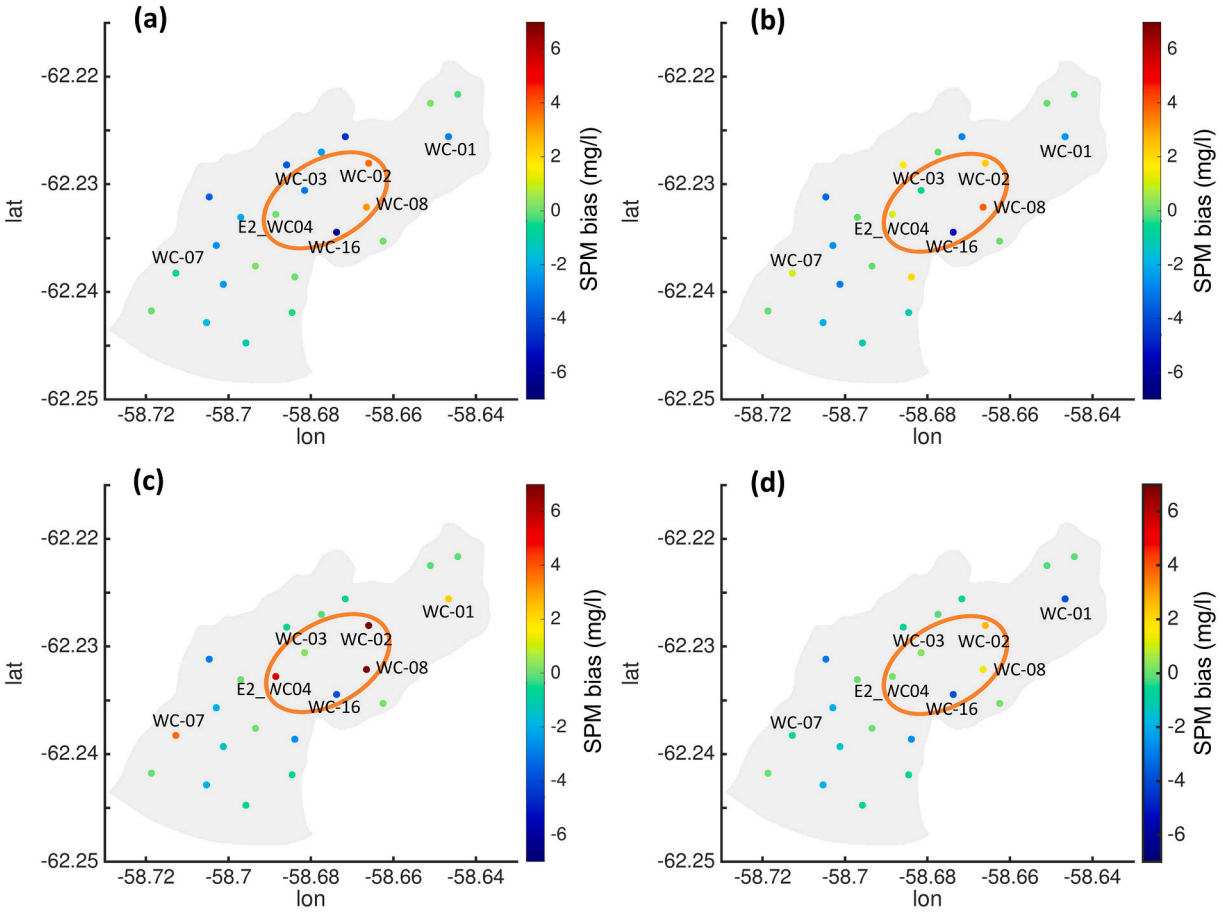

Fig. 10. Model evaluation: the mean difference between simulated and observed SPM concentrations (mg/l) for **(a)** setup 1: only tidal forcing and **(b–d)** setup 2: wind and tidal forcing, **(b)** by default and **(c, d)** Parameterization 2. Note that different results are performed when **(d)** 31st of January measurements are excluded.

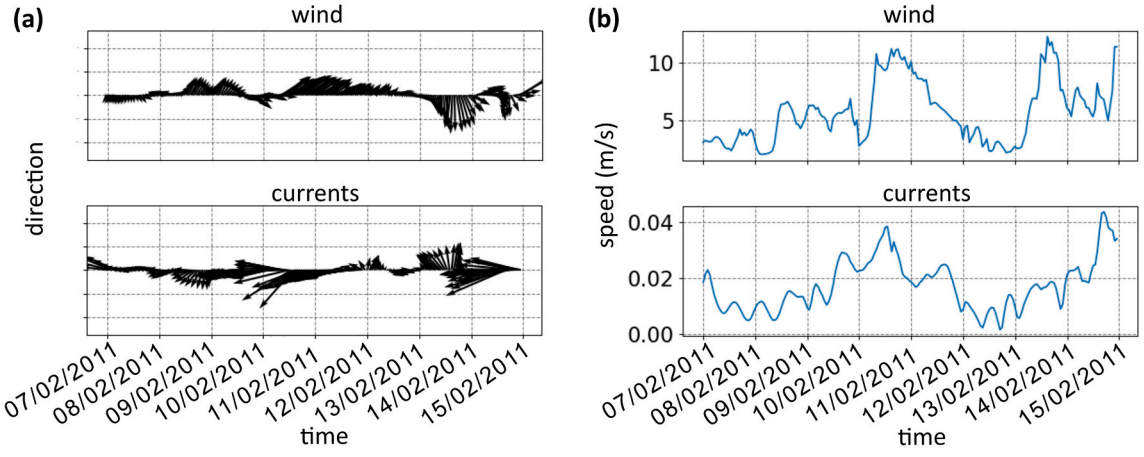

Fig. 11. Wind forcing and currents **(a)** direction and **(b)** speed at different days in February 2011 with a simulated underestimated (9th February) and overestimated (14th February) suspended particulate matter concentration. Between 8th to 10th February the wind direction from the northeast changes to the southeast increasing the speed, revealing the intensity of current velocities. Moreover, a rapid change in wind direction was observed between13th and 14th February after midday, six times the wind speed, modifying the currents.

areas streams. Atmospheric and tidal forcing was considered to simulate circulation pattern and SPM dynamics. The results also provide a valuable baseline for further interdisciplinary research (e.g., species distribution modelling, larvae transport for colonisation predictions, contaminants residence time, etc.) related to SPM distribution and ecosystem dynamics. This study allowed a detailed explanation of the SPM distribution in space and time highlighted by a video of SPM dynamics from 1st December 2010 to 31st March 2011 (Fig. 8b, Video S2). At the beginning of the analysed period, the SPM plume (>15 mg/l) extends mainly in the inner cove, provoking a maximum monthly average SPM concentration and plume extension in February. However, at the end of the period, in March 2010, the plume extension is similar to December 2010 extension covering the inner cove as far as moraine 2. Differences in the simulations are limited by the particle characteristics

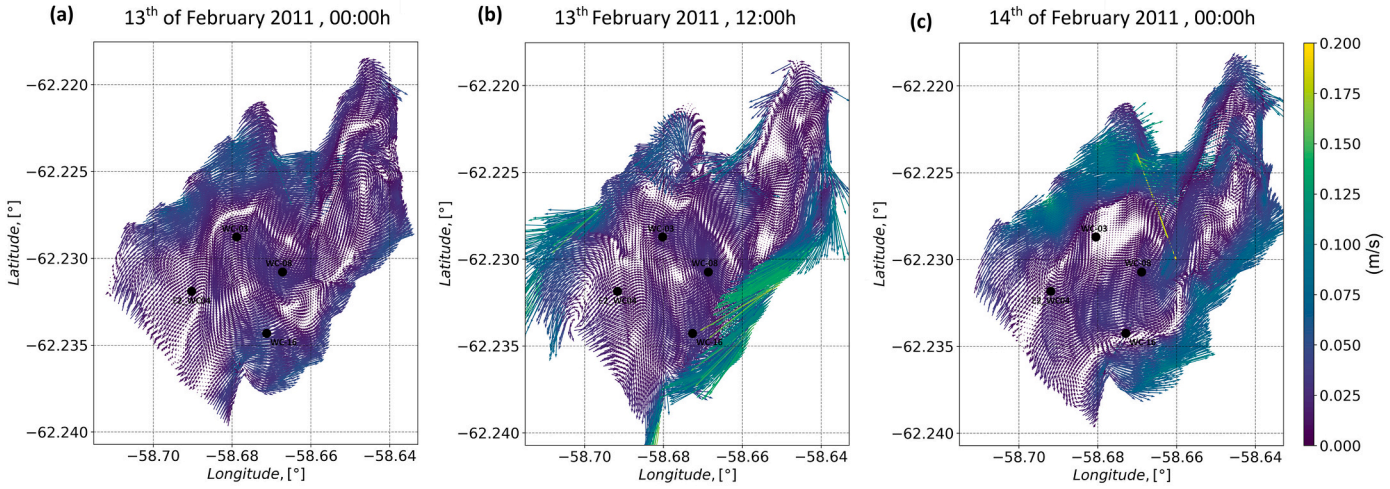

Fig. 12. Average current velocities at different times of days in February 2011 with a simulated overestimated suspended particulate matter concentration.

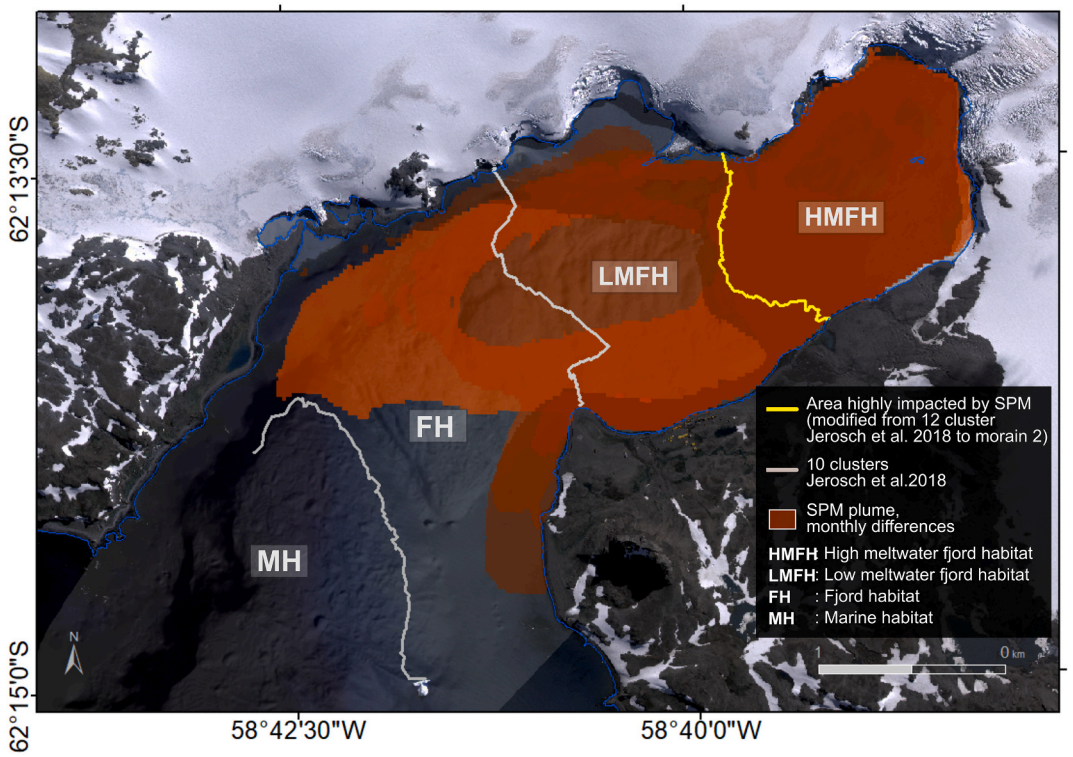

Fig. 13. Fjord habitats in Potter Cove modified from Jerosch et al. (2018) in agreement with the monthly suspended particulate matter (SPM) plume expansion (SPM >15 mg/l) as a relation to meltwater influence. Note the different brown colours are due to overlap on the extension along the other months. (For interpretation of the references to colour in this figure legend, the reader is referred to the web version of this article.)

and defined parameterization, showing that particles in the water column could consist of conglomerates of various densities and diameter sizes. As a post-processing analysis, the Lagrangian tracking module shows the idealised transport dynamics of passive particles from the meltwater streams and glacier sub-catchments. Particles are retained in the inner cove for a maximum of 15 days being exported after 17 days. If specific particle characteristics are further given, the transport trajectories would also allow us to comprehend the fate of not only suspended particulate matter but also nutrients such as dissolved iron or silica, surface-derived food (Jansen et al., 2018), or even possible contaminants as microplastics or metals (Sparaventi et al., 2021) from the terrestrial inputs. Potter Cove is one of many fjords at the tip of the Antarctic Peninsula under atmospheric and ocean warming attributed to anthropogenic factors (IPCC, 2019; Meredith et al., 2019). Increases in ocean temperature show a north-south gradient accompanied by accelerated glacier retreat and ice thinning (Cook et al., 2005, 2016; Vaughan et al., 2013). The FESOM-C model successfully applied to SPM spatial-temporal distribution in Potter Cove can be an exemplary study for other fjordic ecosystems under the impacts of increasing sediment loads associated with glacial melt and other climate-change driven processes.

Declaration of Competing Interest

The authors declare that they have no known competing financial interests or personal relationships that could have appeared to influence

the work reported in this paper.

Acknowledgement

This project was partly supported by Consejo Nacional de Investigaciones Científicas y Técnicas (CONICET-Res. N° 4252/116), by Deutscher Akademischer Austauschdienst (DAAD) and Ministerio de Educación Argentina with the grant ALEARG'18 (ref N° 91700957), by the Alfred Wegener Institute-Helmholtz Center for Polar and Marine Research (AWI), and has received funding from the European Union's Horizon 2020 research and innovation programme under the Marie Skłodowska-Curie grant agreement No 872690 CoastCarb. The authors gratefully acknowledge the provision of tidal data from Potter Cove by Oscar Gonzalez and Martin Roese of the Instituto Antártico Argentino (IAA). Thanks to Dr. Donata Monien and Dr. Patrick Monien for supplying SPM and geological data for Potter Cove. We dedicate this paper to Dr. Doris Abele, who bravely fought a long illness throughout this project. This modelling work draws from the large data pool archived by the previous projects at Potter Cove, BMBF-project IMCOAST, and EU-project IMCONet (FP7 IRSES, action no. 318718). We thank the anonymous reviewer and the Co-Editor, Eileen Hofmann for the positive and constructive comments on the manuscript. Thomas F. Mumford carried out the language editing. Open access was supported by Library OA AWI and Coastal Ecology section.

Appendix A. Supplementary data

Supplementary data to this article can be found online at https://doi.org/10.1016/j.jmarsys.2022.103734.

References

Abele, D., Vasquez, S., Buma, A.G.J., Hernandez, E., 2017. Pelagic and benthic communities of the Antarctic ecosystem of Potter Cove: genomics and ecological implications. Mar. Genomics 33, 1–11. https://doi.org/10.1016/j.margen.2017.05.001.

Ahn, I.Y., Moon, H.W., Jeon, M., Kang, S.H., 2016. First record of massive blooming of benthic diatoms and their association with megabenthic filter feeders on the shallow seafloor of an Antarctic Fjord: does glacier melting fuel the bloom? Ocean Sci. J. 51, 273–279. https://doi.org/10.1007/s12601-016-0023-y.

Androsov, A., Fofonova, V., Kuznetsov, I., et al., 2019. FESOM-C v.2: coastal dynamics on hybrid unstructured meshes. Geosci. Model Dev. 12, 1009–1028. https://doi.org/10.5194/gmd-12-1009-2019.

Ardini, F., Bazzano, A., Rivaro, P., et al., 2016. Trace elements in marine particulate and surface sediments of Kongsfjorden, Svalbard Islands. Rend. Fis. Acc. Lincei 27, 183–190. https://doi.org/10.1007/s12210-016-0524-8.

Barnes, D.K.A., Peck, L.S., 2008. Vulnerability of Antarctic shelf biodiversity to predicted regional warming. Clim. Res. 37 (Epica 2004), 149–163. https://doi.org/10.3354/cr00760.

Barnes, D.K.A., Sands, C.J., Cook, A., Howard, F., Roman Gonzalez, A., Muñoz–Ramirez, C., Retallick, K., Scourse, J., van Landeghem, K., Zwerschke, N., 2020. Blue carbon gains from glacial retreat along Antarctic fjords: what should we expect? Glob. Chang. Biol. 26 (5), 2750–2755. https://doi.org/10.1111/gcb.15055.

Braeckman, U., Pasotti, F., Hoffmann, R., et al., 2021. Glacial melt disturbance shifts community metabolism of an Antarctic seafloor ecosystem from net autotrophy to heterotrophy. Commun. Biol. 4, 1–11. https://doi.org/10.1038/s42003-021-01673-6.

Braun, Matthias Holger, Betsch, Tobias, Seehaus, Thorsten, 2016. King George Island TanDEM-X DEM, Link to GeoTIFF. Institut für Geographie, Friedrich-Alexander-Universität, Erlangen-Nürnberg, PANGAEA. https://doi.org/10.1594/PANGAEA.863567.

Britannica, T. Editors of Encyclopaedia, 2017. Beaufort Scale. Encyclopedia Britannica.

Campana, G.L., Zacher, K., Deregibus, D., et al., 2018. Succession of Antarctic benthic algae (Potter Cove, South Shetland Islands): structural patterns and glacial impact over a four-year period. Polar Biol. 41, 377–396. https://doi.org/10.1007/s00300-017-2197-x.

Clark, G.F., Stark, J.S., Palmer, A.S., Riddle, M.J., Johnston, E.L., 2017. The roles of sea-ice, light and sedimentation in structuring shallow Antarctic benthic communities. PLoS One 12 (1). https://doi.org/10.1371/journal.pone.0168391 e0168391.

Clarke, A., Murphy, E.J., Meredith, M.P., et al., 2007. Climate change and the marine ecosystem of the western Antarctic Peninsula. Philos. Trans. R. Soc. B Biol. Sci. 362, 149–166. https://doi.org/10.1098/rstb.2006.1958.

Cook, A.J., Fox, A.J., Vaughan, D.G., Ferrigno, J.G., 2005. Retreating glacier fronts on the Antarctic Peninsula over the past half-century. Science 308 (5721), 541–544. https://doi.org/10.1126/science.1104235.

Cook, A.J., Holland, P.R., Meredith, M.P., et al., 2016. Ocean forcing of glacier retreat in the western Antarctic Peninsula. Science 353 (80), 283–286.

Danilov, S., Androsov, A., 2015. Cell-vertex discretization of shallow water equations on mixed unstructured meshes. Ocean Dyn. 65, 33–47. https://doi.org/10.1007/s10236-014-0790-x.

Danilov, S., Sidorenko, D., Wang, Q., Jung, T., 2017. Improving the inter-hemispheric gradient of total column atmospheric CO2 and CH4 in simulations with the ECMWF semi-Lagrangian atmospheric global model. Geosci. Model Dev. 10, 1–25. https://doi.org/10.5194/gmd-10-1-2017.

Deregibus, D., Quartino, M.L., Campana, G.L., Momo, F.R., Wiencke, C., Zacher, K., 2016. Photosynthetic light requirements and vertical distribution of macroalgae in newly ice-free areas in Potter Cove, South Shetland Islands, Antarctica. Polar Biol. 39, 153–166. https://doi.org/10.1007/s00300-015-1679-y.

Deregibus, D., Quartino, M.L., Zacher, K., Campana, G., Barnes, D., 2017. Understanding the link between sea ice, ice scours and Antarctic benthic biodiversity-the need for cross-station and international collaboration. Polar Rec. (Gr. Brit.) 53, 143–152. https://doi.org/10.1017/S0032247416000875.

Dierssen, H.M., Smith, R.C., Vernet, M., 2002. Glacial meltwater dynamics in coastal waters west of the Antarctic peninsula. Proc. Natl. Acad. Sci. U. S. A. 99, 1790–1795. https://doi.org/10.1073/pnas.032206999.

DigitalGlobe, 2014. WorldView-2 Scene 103001001F612100, 07/03/2013 under a CC BY License, with Permission from Maxar-EU Space Imaging-DigitalGlobe.

Doxaran, D., Ehn, J., Bélanger, S., Matsuoka, A., Hooker, S., Babin, M., 2012. Optical characterisation of suspended particles in the Mackenzie River plume (Canadian Arctic Ocean) and implications for ocean colour remote sensing. Biogeosciences 9, 3213–3229. https://doi.org/10.5194/bg-9-3213-2012.

Egbert, G.D., Erofeeva, S.Y., 2002. Efficient inverse modeling of barotropic ocean tides. J. Atmos. Ocean. Technol. 19, 183–204.

Falk, U., Silva-Busso, A., 2021. Discharge of groundwater flow to the Potter Cove on King George Island, Antarctic Peninsula. Hydrol. Earth Syst. Sci. 1–24, 3227–3244. https://doi.org/10.5194/hess-25-3227-2021.

Falk, U., Gieseke, H., Kotzur, F., Braun, M., 2016. Monitoring snow and ice surfaces on King George Island, Antarctic Peninsula, with high-resolution TerraSAR-X time series. Antarct. Sci. 28, 135–149. https://doi.org/10.1017/S0954102015000577.

Falk, U., López, D.A., Silva-Busso, A., 2018a. Multi-year analysis of distributed glacier mass balance modelling and equilibrium line altitude on King George Island, Antarctic Peninsula. Cryosphere 12, 1211–1232. https://doi.org/10.5194/tc-12-1211-2018.

Falk, U., Silva-Busso, A., Pölcher, P., 2018b. A simplified method to estimate the run-off in periglacial creeks: a case study of King George Islands, Antarctic Peninsula. Philos. Trans. R. Soc. A Math. Phys. Eng. Sci. 376, 20170166. https://doi.org/10.1098/rsta.2017.0166.

Fettweis, M., Nechad, B., Van den Eynde, D., 2007. An estimate of the suspended particulate matter (SPM) transport in the southern North Sea using SeaWiFS images, in situ measurements and numerical model results. Cont. Shelf Res. 27, 1568–1583. https://doi.org/10.1016/j.csr.2007.01.017.

Fofonova, V., Androsov, A., Sander, L., et al., 2019. Nonlinear aspects of the tidal dynamics in the Sylt-Rømø Bight, southeastern North Sea. Ocean Sci. 15, 1761–1782. https://doi.org/10.5194/os-15-1761-2019.

Fofonova, V., Kärnä, T., Klingbeil, K., Androsov, A., Kuznetsov, I., Sidorenko, D., Danilov, S., Burchard, H., Wiltshire, K.H., 2021. Plume spreading test case for coastal ocean models. Geosci. Model Dev. https://doi.org/10.5194/gmd-2020-438. Discuss. [preprint].

Friedlander, A.M., Goodell, W., Salinas-de-leo, P., Ballesteros, E., Berkenpas, E., Capurro, A.P., Cárdenas, C.A., Hüne, M., Lagger, C., Landaeta, M.F., Muñoz, A., Santos, M., Turchik, A., Werner, R., Sala, E., 2020. Spatial patterns of continental shelf faunal community structure along the Western Antarctic Peninsula. PLoS One 15. https://doi.org/10.1371/journal.pone.0239895 e0239895.

Fuentes, V., Alurralde, G., Meyer, B., Aguirre, G.E., Canepa, A., Wölfl, A., Hass, H.C., Williams, G.N., 2016. Glacial melting: an overlooked threat to Antarctic krill. Sci. Rep. 6, 1–12. https://doi.org/10.1038/srep27234.

Garcia, M.D., Fernández Severini, M.D., Spetter, C., López Abbate, M.C., Tartara, M.N., Nahuelhual, E.G., Marcovecchio, J.E., Schloss, I.R., Hoffmeyer, M.S., 2019. Effects of glacier melting on the planktonic communities of two Antarctic coastal areas (Potter Cove and Hope Bay) in summer. Reg. Stud. Mar. Sci. 30, 100731. https://doi.org/10.1016/j.rsma.2019.100731.

Gutt, J., Isla, E., Xavier, J.C., Adams, B.J., Ahn, I.-Y., Cheng, C.-H.C., et al., 2021. Antarctic ecosystems in transition – life between stresses and opportunities. Biolog. Rev. 96 (3), 798–821. https://doi.org/10.1111/brv.12679.

Hoegh-Guldberg, O., Bruno, J.F., 2010. The impact of climate change on the world's marine ecosystems. Science (New York, N.Y.) 328 (5985), 1523–1528. https://doi.org/10.1126/science.1189930.

Howe, J.A., Austin, W.E.N., Forwick, M., et al., 2010. Fjord systems and archives: a review. Geol. Soc. London Spec. Publ. 344, 5–15. https://doi.org/10.1144/SP344.2.

IPCC, 2019. In: Pörtner, H.-O., Roberts, D.C., Masson-Delmotte, V., Zhai, P., Tignor, M., Poloczanska, E., Mintenbeck, K., Alegría, A., Nicolai, M., Okem, A., Petzold, J., Rama, B., Weyer, N.M. (Eds.), IPCC Special Report on the Ocean and Cryosphere in a Changing Climate. https://www.ipcc.ch/srocc/download-report-2/.

Jansen, J., Hill, N.A., Dunstan, P.K., et al., 2018. Abundance and richness of key Antarctic seafloor fauna correlates with modelled food availability. Nat. Ecol. Evol. 2, 71–80. https://doi.org/10.1038/s41559-017-0392-3.

Jerosch, K., Scharf, F.K., Deregibus, D., et al., 2015. High-resolution bathymetric compilation for Potter Cove, WAP, Antarctica, with links to data in ArcGIS format. PANGAEA. https://doi.org/10.1594/PANGAEA.853593.

Jerosch, K., Pehlke, H., Scharf, F., et al., 2018. Benthic meltwater fjord habitats formed by rapid glacier recession on King Subject Areas : author for correspondence. Philos. Trans. R. Soc. A 376, 20170.
Jerosch, K., Scharf, F.K., Deregibus, D., et al., 2019. Ensemble modeling of Antarctic macroalgal habitats exposed to glacial melt in a Polar Fjord. Front. Ecol. Evol. 7, 207. https://doi.org/10.3389/fevo.2019.00207.
King, M.A., Padman, L., 2005. Accuracy assessment of ocean tide models around Antarctica. Geophys. Res. Lett. 32 https://doi.org/10.1029/2005GL023901. L23608.
Klöser, H., Ferreyra, G.A., Schloss, I.R., et al., 1994. Hydrography of Potter Cove, a small fjord-like inlet on King George Island (South Shetlands). Estuar. Coast. Shelf Sci. 38, 523–537.
Kuznetsov, I., Androsov, A., Fofonova, V., Danilov, S., 2020. Evaluation and application of newly designed finite volume coastal model FESOM-C, effect of variable resolution in the Southeastern North Sea. Water 12, 5. https://doi.org/10.3390/w12051412.
Lagger, C., Servetto, N., Torre, L., Sahade, R., 2017. Benthic colonization in newly ice-free soft-bottom areas in an Antarctic fjord. PLoS One 12. https://doi.org/10.1371/journal.pone.0186756 e0186756.
Lagger, C., Nime, M., Torre, L., et al., 2018. Climate change, glacier retreat and a new ice-free island offer new insights on Antarctic benthic responses. Ecography (Cop) 40, 1–12. https://doi.org/10.1111/ecog.03018.
Lagger, C., Neder, C., Merlo, P., Servetto, N., Jerosch, K., Sahade, R., 2021. Tidewater glacier retreat in Antarctica: the table is set for fast-growing opportunistic species, is it? Estuar. Coast. Shelf Sci. 260, 107447. https://doi.org/10.1016/j.ecss.2021.107447.
Lim, C.H., 2014. Thesis Modelling Waves and Currents in Potter Cove, Antarctica. Fakultät für Mathematik und Naturwissenschaften der Carl von Ossietzky Universität Oldenburg.
Marshall, J., Hill, C., Perelman, L., Adcroft, A., 1997. Hydrostatic, quasi-hydrostatic, and nonhydrostatic ocean modeling. J. Geophys. Res. 102, 5733–5752.
Martinez, M., 2021. A Molecular View on Adaptation on Local and Continental Scales in the Sub-Antarctic and Antarctic Bivalve Aequiyoldia. Doctoral dissertation. Universität Bremen. https://doi.org/10.26092/elib/1142.
Meredith, M.P., Falk, U., Valeria, A., et al., 2018. Anatomy of a glacial meltwater discharge event in an Antarctic cove. Philos. Trans. R. Soc. A Math. Phys. Eng. Sci. https://doi.org/10.1098/rsta.2017.0163.
Meredith, M.P., Sommerkorn, M., Cassotta, S., Derksen, C., Ekaykin, A., Hollowed, A., Kofinas, G., Mackintosh, A., Melbourne-Thomas, J., Muelbert, M.M.C., Ottersen, G., Pritchard, H., Schuur, E.A.G., 2019. Polar regions. In: Pörtner, H.-O., Roberts, D.C., MassonDelmotte, V., Zhai, P., Tignor, M., Poloczanska, E., Nicolai, M., Okem, A., Petzold, J., Rama, B., Weyer, N. (Eds.), IPCC (2019) Special Report on the Ocean and Cryosphere in a Changing Climate. https://www.ipcc.ch/srocc/download-report-2/.
Monien, D., Monien, P., Brünjes, R., et al., 2017. Meltwater as a source of potentially bioavailable iron to Antarctica waters. Antarct. Sci. 29, 277–291. https://doi.org/10.1017/S095410201600064X.
Moon, H.-W., Wan Hussin, W.M.R., Kim, H.-C., Ahn, I.-Y., 2015. The impacts of climate change on Antarctic nearshore mega-epifaunal benthic assemblages in a glacial fjord on King George Island: responses and implications. Ecol. Indic. 57, 280–292. https://doi.org/10.1016/j.ecolind.2015.04.031.
Neder, C., Jerosch, K., Monien, D., et al., 2016. Suspended particulate matter (SPM) and meteorological data in Potter Cove (74 stations), Carlini Station, King George Island (Isla 25 de Mayo) of 21 years German-Argentinian cooperation (1992-2013) compiled within IMCONet. PANGAEA. https://doi.org/10.1594/PANGAEA.871275.
Neder, C., Sahade, R., Abele, D., et al., 2020. Default versus configured-geostatistical modeling of suspended particulate matter in Potter Cove, West Antarctic Peninsula. Fluids 5, 235. https://doi.org/10.3390/fluids504023.
Pasotti, F., Manini, E., Giovannelli, D., et al., 2015. Antarctic shallow water benthos in an area of recent rapid glacier retreat. Mar. Ecol. 36, 716–733. https://doi.org/10.1111/maec.12179.
Philipp, E.E.R., Husmann, G., Abele, D., 2011. The impact of sediment deposition and iceberg scour on the Antarctic soft shell clam Laternula elliptica at King George Island, Antarctica. Antarct. Sci. 23, 127–138. https://doi.org/10.1017/S0954102010000970.
Pineda-Metz, S.E.A., Isla, E., Gerdes, D., 2019. Benthic communities of the Filchner region (Weddell Sea, Antarctica). Mar. Ecol. Prog. Ser. 628, 37–54. https://doi.org/10.3354/meps13093.
Roese, M., 1998. Tesis Aspectos de la circulación en Caleta Potter, Islas Shetland del Sur, Antártida. ITBA-OC-51.00-0004.
Rückamp, M., Braun, M., Suckro, S., Blindow, N., 2011. Observed glacial changes on the King George Island ice cap, Antarctica, in the last decade. Glob. Planet. Chang. 79, 99–109. https://doi.org/10.1016/j.gloplacha.2011.06.009.
Ruiz Barlett, E., Sierra, M.E., Costa, A.J., Tosonotto, G.V., 2021. Interannual variability of hydrographic properties in Potter Cove during summers between 2010 and 2017. Antarct. Sci. 20, 1–20. https://doi.org/10.1017/S0954102020000668.
Sahade, R., Lagger, C., Momo, F.R., et al., 2015. Climate change, glacier retreat drive shifts in an Antarctic benthic ecosystem. Sci. Adv. 1 (10) https://doi.org/10.1126/sciadv.1500050 e1500050.
Schloss, I.R., Ferreyra, G.A., 2002. Primary production, light and vertical mixing in Potter Cove, a shallow bay in the maritime Antarctic. Polar Biol. 25, 41–48. https://doi.org/10.1007/s003000100309.
Schloss, I.R., Klöser, H., Ferreyra, G.A., Curtosi, A., Mercuri, G., Pinola, E., 1997. Factors governing phytoplankton and particulate matter variation in Potter Cove, King George Island, Antarctica. Antarct. Communities 135–141.
Schloss, I.R., Ferreyra, G.A., Mercuri, G., Kowalke, J., 1999. Particle Flux in an Antarctic Shallow Coastal Environment: A Sediment Trap Study, 63, pp. 99–111.
Schloss, I.R., Abele, D., Moreau, S., et al., 2012. Response of phytoplankton dynamics to 19-year (1991–2009) climate trends in Potter Cove (Antarctica). J. Mar. Syst. 92, 53–66. https://doi.org/10.1016/j.jmarsys.2011.10.006.
Schloss, I.R., Wasilowska, A., Dumont, D., Almandoz, G.O., Hernando, M.P., Michaud-Tremblay, C.A., Saravia, L., Rzepecki, M., Monien, P., Monien, D., Kopczyńska, E.E., Bers, A.V., Ferreyra, G.A., 2014. On the phytoplankton bloom in coastal waters of southern King George Island (Antarctica) in January 2010: an exceptional feature? Limnol. Oceanogr. 59, 195–210. https://doi.org/10.4319/lo.2014.59.1.0195.
Schofield, O., Ducklow, H.W., Martinson, D.G., Meredith, M.P., Moline, M.A., Fraser, W. R., 2010. How do polar marine ecosystems respond to rapid climate change? Science (New York, N.Y.) 328 (5985), 1520–1523. https://doi.org/10.1126/science.1185779.
Servicio Nacional Meteorológico, 2019. Reporte mediciones antárticas Expediente175494. Gobierno de la Nación Argentina.
Siciński, J., Pabis, K., Jażdżewski, K., Konopacka, A., Błażewicz-Paszkowycz, M., 2012. Macrozoobenthos of two Antarctic glacial coves: a comparison with non-disturbed bottom areas. Polar Biol. 35 (3), 355–367. https://doi.org/10.1007/s00300-011-1081-3.
Simpson, G., Castelltort, S., 2006. Coupled model of surface water flow, sediment transport and morphological evolution. Comput. Geosci. 32, 1600–1614. https://doi.org/10.1016/j.cageo.2006.02.020.
Slattery, M., Bockus, D., 1997. Sedimentation in McMurdo Sound, Antarctica: a disturbance mechanism for benthic invertebrates. Polar Biol. 18 (3), 172–179. https://doi.org/10.1007/s003000050174.
Smale, D.A., Brown, K.M., Barnes, D.K.A., Fraser, K.P.P., Clarke, A., 2008. Ice scour disturbance in Antarctic waters. Science 321 (5887), 371. https://doi.org/10.1126/science.1158647.
Sparaventi, E., Rodríguez-Romero, A., Barbosa, A., Ramajo, L., Tovar-Sánchez, A., 2021. Trace elements in Antarctic penguins and the potential role of guano as source of recycled metals in the Southern Ocean. Chemosphere 285, 131423. https://doi.org/10.1016/j.chemosphere.2021.131423.
Thrush, S.F., Hewitt, J.E., Cummings, V.J., Ellis, J.I., Hatton, C., Lohrer, A., Norkko, A., 2004. Muddy Waters : Elevating Sediment Input to Coastal and Estuarine Habitats.
Torre, L., Servetto, N., Eöry, M.L., Momo, F., Tatián, M., Abele, D., Sahade, R., 2012. Respiratory responses of three Antarctic ascidians and a sea pen to increased sediment concentrations. Polar Biol. 35, 1743–1748. https://doi.org/10.1007/s00300-012-1208-1.
Torre, L., Abele, D., Lagger, C., et al., 2014. When shape matters: strategies of different Antarctic ascidians morphotypes to deal with sedimentation. Mar. Environ. Res. 99, 179–187. https://doi.org/10.1016/j.marenvres.2014.05.014.
Torre, L., Tabares, P.C.C., Momo, F., Meyer, J.F.C.A., Sahade, R., 2017. Climate change effects on Antarctic benthos: a spatially explicit model approach. Clim. Chang. 141, 733–746. https://doi.org/10.1007/s10584-017-1915-2.
Torre, L., Alurralde, G., Lagger, C., Abele, D., Schloss, I.R., Sahade, R., 2021. Antarctic ascidians under increasing sedimentation: physiological thresholds and ecosystem hysteresis. Mar. Environ. Res. 167 (February), 105284.
TPXO, 2020. OSU TPXO9-Atlas Latest Version: v4. https://www.tpxo.net/global/tpxo9-atlas.
Turner, J., Lu, H., White, I., King, J.C., Phillips, T., Hosking, J.S., Bracegirdle, T.J., Marshall, G.J., Mulvaney, R., Deb, P., 2016. Absence of 21st century warming on Antarctic Peninsula consistent with natural variability. Nature 535 (7612), 411–415. https://doi.org/10.1038/nature18645.
U.S. Geological Survey, 2019. Landsat 8 Surface Reflectance Code (LASRC) Product Guide (No. LSDS-1368 Version 2.0). 40.
van Rijn, L.C., 1984. Sediment transport, part I: bed load transport. J. Hydraul. Eng. 110, 1431–1456.
van Rijn, L.C., 1985. Sediment transport. Part 2 Suspended load transport. J. Hydraul. Eng. 110, 1613–1641.
van Rijn, L.C., 1987. Mathematical Modelling of Morphological Processes in the Case of Suspended Sediment Transport.
Vaughan, D.G., Comiso, J.C., Allison, I., et al., 2013. Observations: Cryosphere supplementary material. In: Stocker, T.F., Qin, D., Plattner, G.-K., et al. (Eds.), Climate Change 2013: The Physical Science Basis. Contribution of Working Group I to the Fifth Assessment Report of the Inter-governmental Panel on Climate Change. IPCC. www.climatechange2013.org.
Wlodarska-Kowalczuk, M., Pearson, T.H., Kendall, M.A., 2005. Benthic response to chronic natural physical disturbance by glacial sedimentation in an Arctic fjord. Mar. Ecol. Prog. Ser. 303 (Hall 1994), 31–41.
Yoo, K., Kyung Lee, M., Il Yoon, H., Il Lee, Y., Yoon Kang, C., 2015. Hydrography of Marian Cove, King George Island, West Antarctica: implications for ice-proximal sedimentation during summer. Antarct. Sci. 27 (2), 185–196. https://doi.org/10.1017/S095410201400056X.
Zacher, K., Wulff, A., Molis, M., Hanelt, D., Wiencke, C., 2007. Ultraviolet radiation and consumer effects on a field-grown intertidal macroalgal assemblage in Antarctica. Glob. Chang. Biol. 13, 1201–1215. https://doi.org/10.1111/j.1365-2486.2007.01349.x.
Zentek, R., Heinemann, G., 2020. Verification of the regional atmospheric model CCLM v5. 0 with conventional data and lidar measurements in Antarctica. Geosci. Model Dev. 13 (4), 1809–1825. https://doi.org/10.5194/gmd-13-1809-2020.
Zwerschke, N., Morley, S.A., Peck, L.S., Barnes, D.K.A., 2021. Can Antarctica's shallow zoobenthos 'bounce back' from iceberg scouring impacts driven by climate change? Glob. Chang. Biol. 1–9. https://doi.org/10.1111/gcb.15617. January.